

AD-A175 756

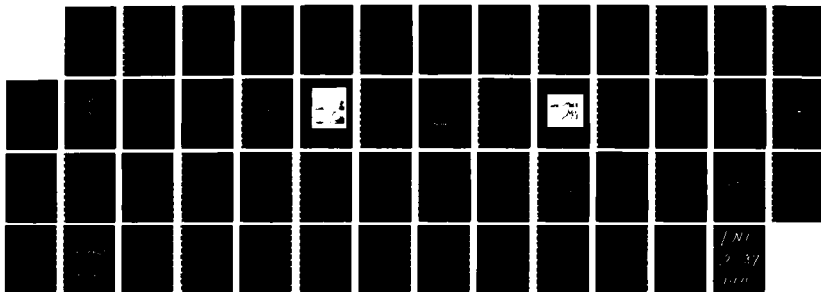
KINETIC MODEL OF AURORAL PLASMA FORMATION II:
SIMULTANEOUS MULTI-SATELLIT (U) AEROSPACE CORP EL
SEGUNDO CA SPACE SCIENCES LAB Y T CHIU ET AL

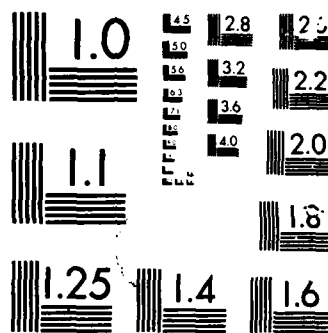
1/1

UNCLASSIFIED

30 SEP 86 TR-0086(6940-05)-4 SD-TR-86-69 F/G 4/1

NL





12

AD-A175 756

Kinetic Model of Auroral Plasma Formation II: Simultaneous Multi-Satellite Ion Observations and Interpretations

Y. T. CHIU and O. W. LENNARTSSON
Lockheed Palo Alto Research Laboratories
Palo Alto, CA 94304

A. KORTH and G. KREMSER
Max Planck Institut fur Aeronomie
Lindau, West Germany

and

J. F. FENNELL and A. M. KISHI
Space Sciences Laboratory
Laboratory Operations
The Aerospace Corporation
El Segundo, CA 90245

30 September 1986

Prepared for
SPACE DIVISION
AIR FORCE SYSTEMS COMMAND
Los Angeles Air Force Station
P.O. Box 92960, Worldway Postal Center
Los Angeles, CA 90009-2960

DTIC FILE COPY

APPROVED FOR PUBLIC RELEASE;
DISTRIBUTION UNLIMITED

DTIC
JAN 6 1987
A

This report was submitted by The Aerospace Corporation, El Segundo, CA 90245, under Contract No. F04701-85-C-0086 with the Space Division, P.O. Box 92960, Worldway Postal Center, Los Angeles, CA 90009-2960. It was reviewed and approved for The Aerospace Corporation by H. R. Rugge, Director, Space Sciences Laboratory.

Capt. Douglas R. Case/YCM was the project officer for the Mission-Oriented Investigation and Experimentation (MOIE) Program.

This report has been reviewed by the Public Affairs Office (PAS) and is releasable to the National Technical Information Service (NTIS). At NTIS, it will be available to the general public, including foreign nationals.

This technical report has been reviewed and is approved for publication. Publication of this report does not constitute Air Force approval of the report's findings or conclusions. It is published only for the exchange and stimulation of ideas.



DOUGLAS R. CASE, Capt, USAF
MOIE Project Officer
SD/YCM



JOSEPH HESS, GM-15
Director, AFSTC West Coast Office
AFSTC/WCO OL-AB

UNCLASSIFIED

SECURITY CLASSIFICATION OF THIS PAGE (When Data Entered)

REPORT DOCUMENTATION PAGE		READ INSTRUCTIONS BEFORE COMPLETING FORM
1. REPORT NUMBER SD-TR-86-69	2. GOVT ACCESSION NO.	3. RECIPIENT'S CATALOG NUMBER
4. TITLE (and Subtitle) KINETIC MODEL OF AURORAL PLASMA FORMATION II: SIMULTANEOUS MULTI-SATELLITE ION OBSERVATIONS AND INTERPRETATIONS		5. TYPE OF REPORT & PERIOD COVERED
		6. PERFORMING ORG. REPORT NUMBER TR-0086(6940-05)-4
7. AUTHOR(s) Y. T. Chiu, O. W. Lennartsson, A. Korth, G. Kremser, Joseph F. Fennell, and Arlene M. Kishi		8. CONTRACT OR GRANT NUMBER(s) F04701-85-C-0086
9. PERFORMING ORGANIZATION NAME AND ADDRESS The Aerospace Corporation El Segundo, CA 90245		10. PROGRAM ELEMENT, PROJECT, TASK AREA & WORK UNIT NUMBERS
11. CONTROLLING OFFICE NAME AND ADDRESS Space Division Los Angeles Air Force Station Los Angeles, CA 90009-2960		12. REPORT DATE 30 September 1986
		13. NUMBER OF PAGES 47
14. MONITORING AGENCY NAME & ADDRESS (if different from Controlling Office)		15. SECURITY CLASS. (of this report) Unclassified
		15a. DECLASSIFICATION/DOWNGRADING SCHEDULE
16. DISTRIBUTION STATEMENT (of this Report) Approved for public release; distribution unlimited.		
17. DISTRIBUTION STATEMENT (of the abstract entered in Block 20, if different from Report)		
18. SUPPLEMENTARY NOTES		
19. KEY WORDS (Continue on reverse side if necessary and identify by block number) Auroral Plasma Magnetosphere Geosynchronous Orbit Particle Kinetics Ion Convection Substorm		
20. ABSTRACT (Continue on reverse side if necessary and identify by block number) A detailed analysis of ion composition and distribution observed simultaneously by GEOS-II, SCATHA, and ISEE-I satellites at the initial phase of an injection event in the inner magnetosphere on March 22, 1979, has been made. The mean convection electric field observed by GEOS-II during the data interval (10:00-14:00 UT) was used to determine the space-time variation of a global time-dependent convection electric field model [Chiu and Kishi, 1984], which is approximately verified in this report by		

DD FORM 1473
(FACSIMILE)UNCLASSIFIED
SECURITY CLASSIFICATION OF THIS PAGE (When Data Entered)

UNCLASSIFIED

SECURITY CLASSIFICATION OF THIS PAGE(When Data Entered)

19. KEY WORDS (Continued)

20. ABSTRACT (Continued)

ISEE-I plasma flow measurements and by the unusual SCATHA observation of low energy ions convected from the plasmasphere cloak region. Theoretical tracing of ion trajectories with the tested electric field model indicates that multi-satellite observations of keV ion dispersion can be interpreted in terms of a "collision/mixing" between an injected auroral ion population rich in oxygen with a pre-injection population rich in hydrogen and doubly-ionized helium which had previously moved inward from ISEE-I orbit. The results of this "collision/mixing" was that ion dispersion signatures afterwards appeared as if they were from a single population, having lost memory of their previous convection history. ~~We conjecture that this is a~~ possible formation mechanism of the ad hoc injection boundary which is marked only by plasma dispersion signature and not by any other magnetospheric feature.

UNCLASSIFIED

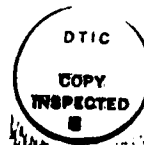
SECURITY CLASSIFICATION OF THIS PAGE(When Data Entered)

PREFACE

We thank J. M. Quinn for analysis of the SCATHA ion composition data and A. Pedersen for providing electric field data from GEOS-II.

CONTENTS

PREFACE.....	1
I. INTRODUCTION.....	7
II. ELECTRIC FIELD DATA AND MODEL.....	9
III. SATELLITE CONSTELLATION AND ION DATA.....	15
IV. THEORETICAL FRAMEWORK.....	25
V. DISCUSSION AND INTERPRETATION.....	33
A. Source of Low Energy Ions.....	33
B. Dispersion of Intermediate and High Energy Ions.....	34
VI. CONCLUSIONS.....	49
REFERENCES.....	51



FIGURES

1.	Sunward and Eastward Electric Field Components Measured at GEOS-II During the Data Period on March 22, 1979 [Knott et al., 1985].....	10
2.	Ion Flow as Measured by the Electrostatic Analyzer Section of the Lockheed Mass Spectrometer on ISEE-I (0.1-16 keV/q).....	12
3.	Plot on the Equatorial Plane Exhibiting the Location of the Satellite Constellation Used in This Study.....	16
4.	Energy-Time Spectrogram of the UCSD Plasma Instrument on Board SCATHA During the Data Interval.....	17
5.	Ion Flux Intensities Measured by the MPAE GEOS-II Instrument in the Data Interval for Two Pitch Angles Highlighting the Two Distinct Dispersion Features.....	19
6.	Energy-Time Spectrogram for Hydrogen and Oxygen Obtained by the Lockheed Mass Spectrometer on Board SCATHA [Strangeway and Johnson, 1983].....	21
7.	Ion Number Densities Measured by the Lockheed Mass Spectrometer on ISEE-I (0.1-16 keV/q).....	22
8.	Hydrogen and Oxygen Energy Spectra Measured for Two Pitch Angles by the Lockheed Instrument on ISEE-I.....	23
9.	Backward Trajectory Traces with Our Convection Potential Model from SCATHA (S) and GEOS-II (G) for Low Energy Ions Represented by Those of 10 eV Initial Energy and 90° Pitch Angle.....	26
10.	Backward Trajectory Traces with Our Convection Potential Model from SCATHA (S) and GEOS-II (G) for Intermediate and High Energy Ions at 90° Pitch Angle and Starting at 11:00 UT.....	27
11.	Same as Figure 10 but for Backward Tracing from 11:30 UT.....	28
12.	Same as Figure 10 but for Backward Tracing from 12:00 UT.....	29
13.	Same as Figure 10 but for Backward Tracing from 13:00 UT.....	30
14.	Same as Figure 5 but for the Remainder of the Complete Set of Pitch Angles.....	36

15. Electron Flux Intensities Measured by the MPAE Instrument on GEOS-II Exhibiting Two Distinct Dispersion Features Which "Merged" at a Later Time, but Within our Data Interval.....	38
16. Temporal Development of Ion Pitch Angle Distributions Measured by the Aerospace Instrument on SCATHA.....	39
17. Flux Intensities of Ions at $90^\circ \pm 10^\circ$ and $0^\circ - 30^\circ$ Pitch Angle Measured by the Aerospace Instrument.....	40
18. Temporal Development of Flux Intensities of Hydrogen and Oxygen Measured by the Lockheed Mass Spectrometer on SCATHA for Two Pitch Angle Bins.....	42

I. INTRODUCTION

The formation of auroral arcs has been the focus of a major segment of magnetospheric research. In recent years important developments of theoretical and experimental consequences have taken place in the area of particle acceleration and arc formation in the $1 R_E$ altitude region. However, underlying these developments which are based on kinetic theory, a basic question needs to be answered: From where and how does the auroral plasma acquire its kinetic characteristics? In an initial attempt to answer this question, we have examined the space-time response of magnetospheric electron distributions to time-dependent electric fields [Chiu and Kishi, 1984; Paper I]. In Paper I, we show that many interesting features of electron distributions associated with auroral plasma injection can be understood in the framework of time response of electron adiabatic transport to sudden changes of magnetospheric electric fields. In our studies, we are concerned with auroral plasma formation; little attempt was made to examine the *ad hoc* injection boundary model [e.g., Mauk and Meng, 1983; McIlwain, 1974] in the light of time-dependent physical processes. Nevertheless, some general features of electron dispersion in the inner magnetosphere were found to be in common with the transient adiabatic response of the plasma to sudden changes in the global electric field. In particular, the convection of such sudden responses into the inner magnetosphere produces electron distribution signatures that qualitatively mimic those expected from the injection boundary hypothesis, except that strong dispersion in pitch angle can result from time dependent transport, as is evident in observations [Koons and Fennell, 1984]. With somewhat different arguments, Fairfield and Vinas [1984] have also concluded that adiabatic transport is the dominant process in the inner magnetosphere.

Here, in the second paper of the series, we turn our attention to the injection of auroral ions and attempt to examine their characteristics under the same time-response theoretical framework as Paper I [Chiu and Kishi, 1984] but with more emphasis upon evolving a physical mechanism for the formation of (or physical effects that imitate the apparent behavior of) the injected plasma. Again, our aim is not to explain the injection boundary hypothesis, but to seek the physical mechanisms that energize and transport plasma during the initial phase of substorms. Thus, instead of mapping particles from an *ad hoc* boundary, we attempt to map particles backwards

in time, proceeding in parallel with the original development of the injection boundary hypothesis [e.g., McIlwain, 1972], but with a model of space-time dependent electric fields and with simultaneous multiple satellite observations. Neither features were available to previous analyses.

Further, realizing that mapping with an assumed space-time dependent electric field with no observational support is fundamentally not more realistic than mapping with an assumed static electric field model, we specifically consider ion injection data for which simultaneous electric field measurements are available to test the model. Since a satellite moves in space-time in a data interval, a time-dependent global electric field model can be constructed from the measurements if the interval is long enough. However, single point measurements in space-time are rather unconstrained in that space and time effects are not easily separable without further assumptions; therefore, we require simultaneous multiple-satellite ion and electric field data sets in order to examine the physical processes associated with auroral plasma formation and injection. Considering the severe restrictions that such a study would place on available data and considering the paucity of electric field measurements on equatorial satellites in the inner magnetosphere [Pedersen et al., 1978], it is surprising that the union of all currently available data sets satisfying the above restrictions is not null. Nevertheless, we have been able to take advantage of data analysis work associated with the CDAW-6 period (March 22, 1979) to examine ion transport data from GEOS-II, ISEE-I, and SCATHA satellites which satisfied all of the above restrictions. We believe that an attempt at theoretical interpretation of detailed particle signatures in the light of measured electric field signatures with a simultaneous multi-satellite data set is absolutely necessary to elucidate the physical processes of plasma injection and energization in the inner magnetosphere. Our work here is probably a first attempt to do so in detail.

II. ELECTRIC FIELD DATA AND MODEL

To study the space-time response of inner magnetospheric ions with a multi-satellite data set, we cannot choose to investigate quiet time mapping since there are no natural demarcations in the quiet-time electric field. We believe that the physics of auroral plasma injection is best examined in its formation stages. Therefore, the best data intervals to study time response are those following distinct increases and/or decreases of the global convection electric field leading eventually to a clear injection event and lasting for durations longer than or comparable to ion transit times through the inner magnetosphere. In such intervals, it is expected that ion response signals will be distinct and be easier to recognize. Examination of the electric field data from GEOS-II in Figure 1 indicates that such a suitable period [Knott et al., 1985] satisfying all constraints is the 10:00-14:00 UT interval on March 22, 1979, a period of relative quiet in the inner magnetospheric particle environment before the injection event commencing at about 14:30 UT. Early in this period, it will be seen that particle injection is clearly taking place, although the bulk of the particles did not arrive at the inner magnetosphere until after 12:00 UT with the usual dispersion. In Figure 1, two changes of average electric field can be identified in this period, although the fluctuating signal is very strong. The AC electric signal has typical periods of 10 min. or so, much longer than the oxygen ion cyclotron period for resonant wave-particle interaction to take place, so we do not expect the AC signal to destroy the assumptions of adiabaticity, which is used not only in our consideration here, but also explicitly in the injection boundary hypothesis. Because of the existence of the AC signal, it must be made clear at the outset that we are dealing with the convection effects of the mean field, which happens to be smaller than the AC field. At 10:08 UT, a mean electric field increase is identified to be coincident with a southward turning of the IMF detected by IMP-8. Later, at about 11:40 UT, the average field is seen to decrease in response to northward turning of the IMF. During this period, the sunward (top panel) and eastward (bottom panel) components of the average field are less than ~ 2 mV/m. Further, prior to this period, since 8:00 UT and including the sudden commencement at about 8:25 UT, the average electric field did not show any significant change.

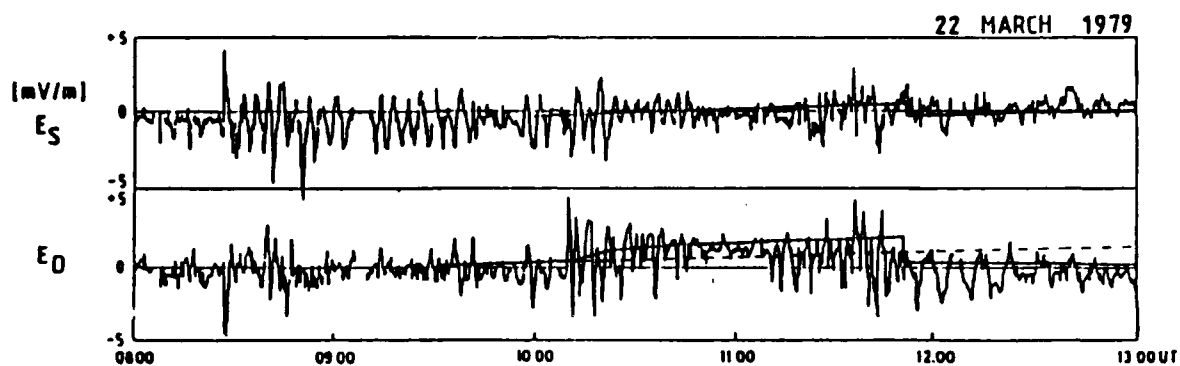


Figure 1. Sunward and Eastward Electric Field Components Measured at GEOS-II During the Data Period on March 22, 1979 [Knott et al., 1985]. The solid lines are results of the convection potential of the present report. The dashed line is the eastward component of electric field from Volland's [1973] model normalized to the present model before the field increase at 10:08 UT.

Since a global time-dependent electric field model has been shown to work quite well for electron distributions in Paper I, an important initial task here is to ask if the model also works for the ion transport case if the time dependence is modified to reflect the sequential increase and decrease of electric fields shown in Figure 1. In a time interval of four hours, the GEOS-II satellite has covered the afternoon quadrant of space with measurements of both sunward and eastward electric field components; hence the data in Figure 1 is a fairly stringent test of the electric field model potential

$$\Phi(L, \varphi, t) = \Phi_c(t) L^2 \sin \varphi + \Phi_o / L \quad (1)$$

where L is the McIlwain parameter, φ is the local time angle measured counter clockwise from noon, and t is time. $\Phi_o \sim -92$ kV is the magnitude of the co-rotational potential, and Φ_c is the time dependent part of the potential modeled by

$$\Phi_c(t) = \Phi^* + \Delta\Phi^* \{1 - \exp[-(t - t_i)/t_i^*]\} \Theta(t - t_i) \{1 + \zeta \Theta(t - t_f)\} \quad (2)$$

The time factor models a jump of the potential from Φ^* to $\Phi^* + \Delta\Phi^*$, initiated at time $t = t_i$, with a rise time, t_i^* . Subsequently, starting at $t \geq t_f$, the potential suddenly decreases to $\Phi^* + \Delta\Phi^*(1 + \zeta)$. Without making a quantitative fit, the following parameter values are chosen on the basis of the field model used in Paper I: $\Delta\Phi^* = 2\Phi^*$, $\Phi^* = -0.5$ kV, $\zeta = -7/6$, $t_i^* = 0.382$ hrs. Solid lines on the two panels of Figure 1 show the modeled electric field components at the location and time of GEOS-II observations. For comparison, the prediction for the eastward electric field from the Volland [1973] potential with magnitude Φ^* is plotted as a dashed curve on Figure 1. Considering that no effort was made to make a formal fit, the comparison shown on Figure 1 is evidence that our global electric field model is a reasonable approximation to reality. The electric field model can be improved by a slight phase rotation in local time, and it would be of interest to have the model results checked by comparison with measurements from another spacecraft. Although SCATHA did not have electric field measurements at the time, ISEE-I plasma flow data are available to us. Figure 2 shows the magnitude and direction in the solar ecliptic plane of the ion flow measured by the ISEE-I mass spectrometer [Shelley et al., 1978], along with the polar and ecliptic angles of the measured magnetic field [Russell, 1978]. This ion flow is a combination of drift motions parallel and perpendicular to the local magnetic field, a combination that partially depends on the polar angle of the

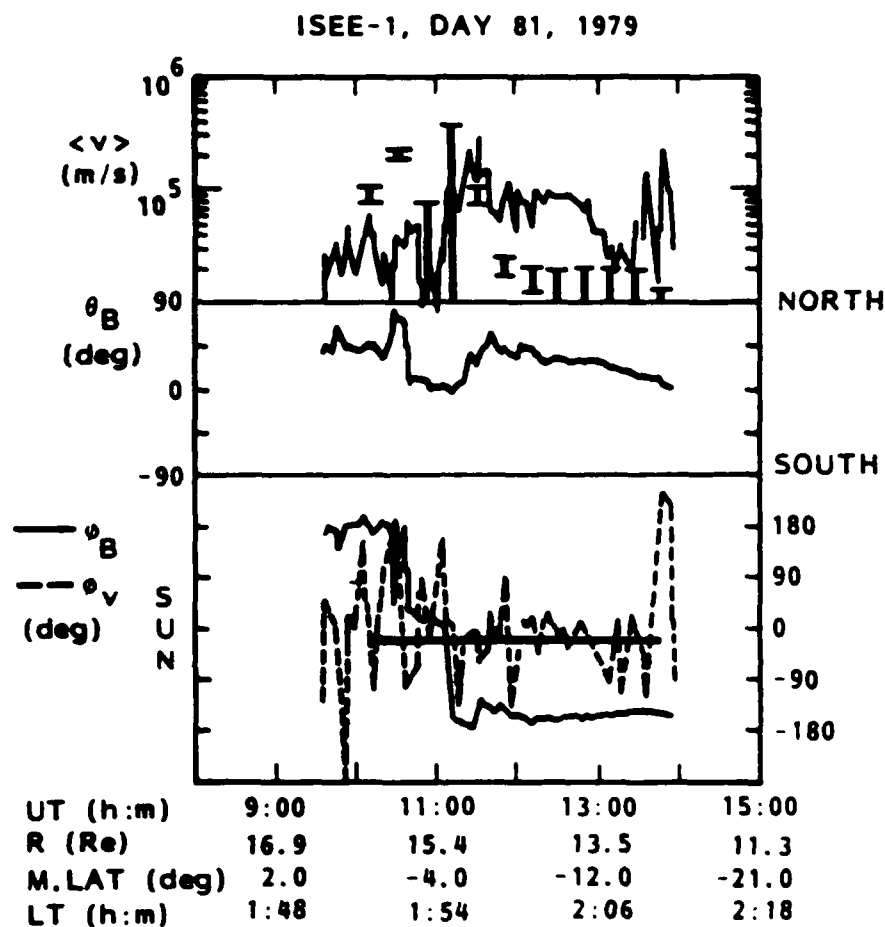


Figure 2. Ion Flow as Measured by the Electrostatic Analyzer Section of the Lockheed Mass Spectrometer on ISEE-1 (0.1-16 keV/q). The flow speed (assuming the total ion flux is dominated by H^+) is shown in the top panel, and the flow angle within the solar ecliptic plane is shown in the bottom panel, measured counterclockwise from noon. The direction of the measured magnetic field is also indicated by a polar angle (middle panel) and an ecliptic angle (bottom panel). The solid bars in the top panel and the horizontal line in the bottom panel are based on predictions by our electric field model.

magnetic field. The mass spectrometer is most sensitive to ions moving within about 0° to -10° polar angle (the ISEE-I spin plane is near 0° polar angle), but the angular acceptance increases with decreasing energy and approaches the range of $+15^\circ$ to -25° at 100 eV/q. Because of the nature of the ion flow measurements and because of the local deviation of the magnetic field from a dipole field (indicated here by rapid angular direction and magnitude variations), we cannot make a strictly valid comparison. However, as a first order approximation, we have taken the electric field vector predicted by our model and calculated an $E \times B$ drift using the measured magnetic field vector. The resulting drift speed at 20 minute intervals is indicated in the top panel of Figure 2 in the form of bars. The top of each bar is the absolute speed, and the bottom of each bar is the projection onto the ecliptic plane. The mass spectrometer would measure a speed somewhere between the top and bottom of each bar, provided there was no field-aligned motion. In view of the circumstances, there is considerable agreement between the predicted and measured flow speeds, at least part of the time. The fact that our predictions lead to consistently low speeds after 11:40 UT (after the reduction of the potential) may be partially due to the inability of our model to account for field-aligned flow. In any case, our model gives a fairly good prediction of the average flow direction in the ecliptic plane, as shown in the bottom panel of Figure 2. Since ISEE-I was near 2 LT at $\sim 15 R_E$ during the data interval, the model-data comparison shown in Figure 2 is a rather stringent test of our simple global time-dependent electric field model. Further, since ISEE-I was clearly upstream of GEOS-II in the sense of the trajectories of injected ions, the test shown on Figure 2 gives us some confidence that our ion trajectories, traced backwards in time, are not far from reality. Ion data interpretations will be based on this electric field model.

III. SATELLITE CONSTELLATION AND ION DATA

In this section, we shall briefly survey the data and scenario chosen for this study. A brief logical sequence is presented, but detailed discussions are deferred to later sections.

The data interval chosen for this study has also the advantage that two spacecrafts (SCATHA and GEOS-II) were approximately aligned along a radial direction from the Earth, both moving in local time from about noon towards dusk, as shown on Figure 3. The radial alignment and locations of the satellites in the afternoon sector are most suitable for studying ions in the 1 - 100 keV energy range, since they convect towards the duskside. Meanwhile, during the data interval, ISEE-I is at $\sim 15 R_E$ and at 2 LT, also near the equatorial plane; thus, it is located upstream of the ion convection flow. Clearly, the satellite constellation during the data interval is well suited for detailed studies of ion sources and transport.

To begin a data description of the event interval, we use the survey particle spectrogram of the University of California at San Diego (UCSD) plasma instrument on SCATHA [e.g., Olsen, 1981], shown on Figure 4. In the interval 10:00-14:00 UT, the most noticeable feature is the strong flux increase of > 30 keV ions just before 12:00 UT. The dispersion of arrival times subsequent to this apparent initiation has been used as argument for the injection boundary model [Strangeway and Johnson, 1984]. We do not disagree with, but endorse, the gross features involved in such an argument. However, to elucidate the physical processes of injection and energization, we must ask whether other features shown on the ion spectrogram of Figure 4 are also consistent with the assumption of a single source. If not, it would be revealing to ask if a physical mechanism can be found to incorporate the consequences of multiple, as well as single, sources in a global model. In the process, we may gain an understanding on the meaning of the injection boundary model (IBM). In short, we neither seek to destroy nor to preserve the hypothesis, but to search for a mechanism of inner-magnetospheric plasma transport that can accommodate as many observed features as possible, without regard to whether they are consequences of any particular hypothesis. In this regard, two important features must be noted in Figure 4. First, intense fluxes of a component of low energy ions were observed to arrive at $\sim 12:00$ UT and afterward, but were clearly not on the expected dispersion curve. Second, careful

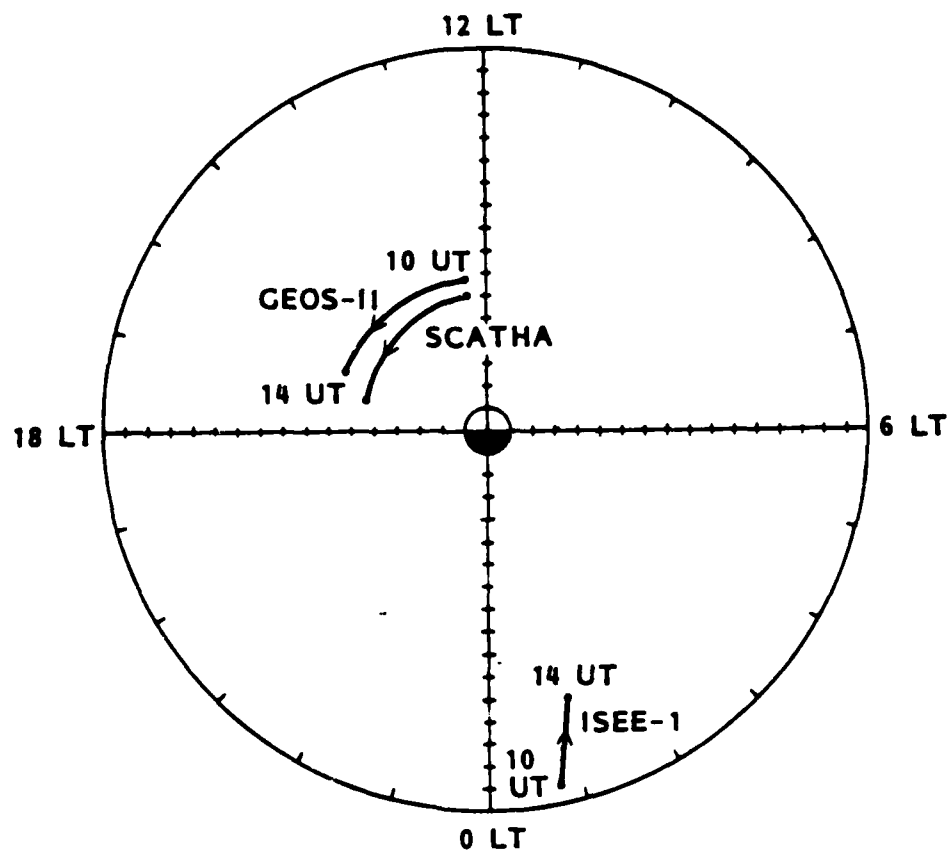


Figure 3. Plot on the Equatorial Plane Exhibiting the Location of the Satellite Constellation Used in This Study. The dark lines span the locations of individual satellites during the data interval (10:00-13:00 UT).

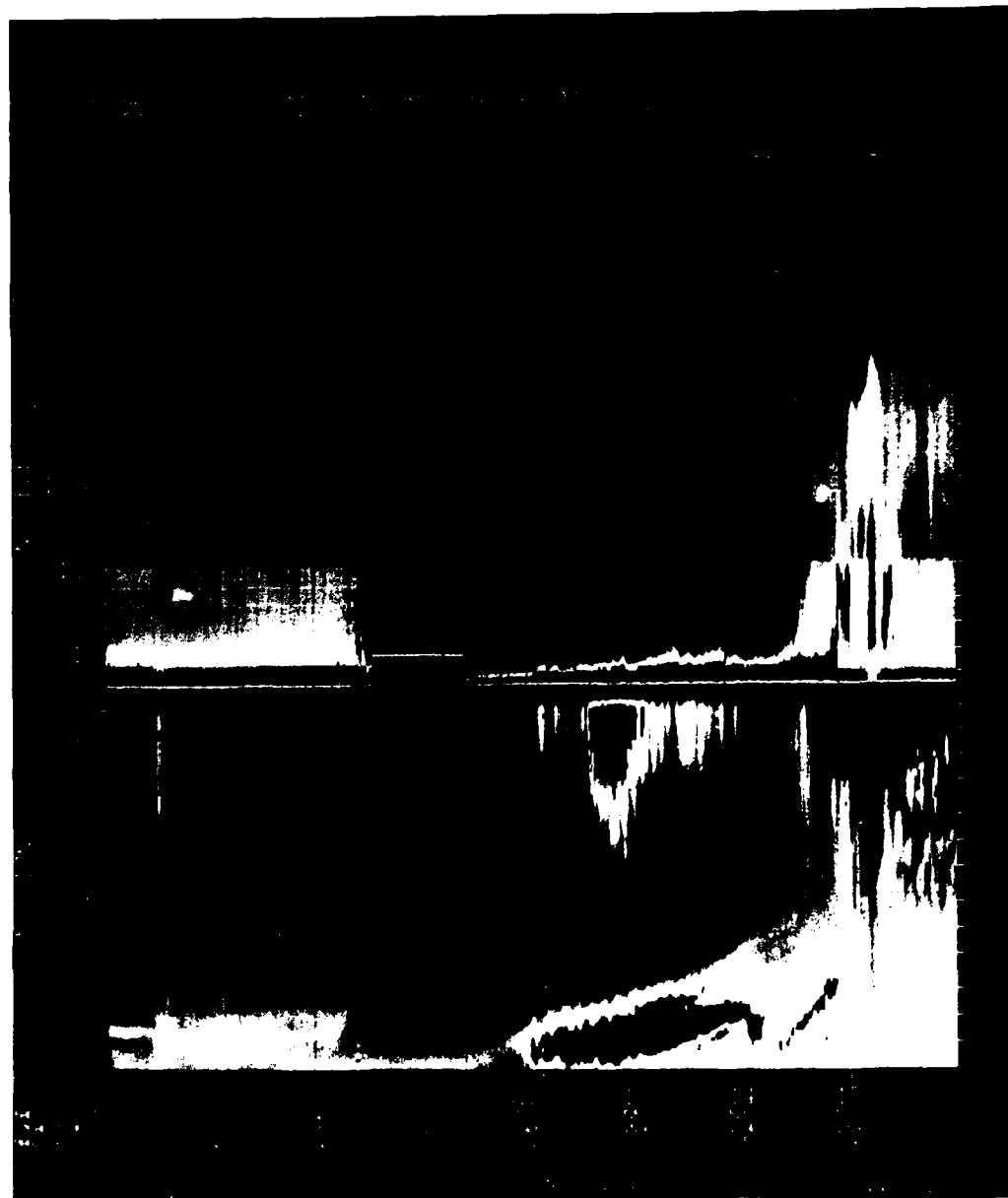


Figure 4. Energy-Time Spectrogram of the UCSD Plasma Instrument on Board SCATHA During the Data Interval. The event after 12:00 UT reveals the characteristic dispersion spanning ions and electrons usually attributed to the ad hoc injection boundary. The low-energy ion component is a notable exception. Our study is limited to the initial phase of the event before 13:00 UT.

examination of the fluxes of energetic ions prior to the simultaneous (dispersionless?) increase at about 12:00 UT shows that they started increasing almost a half hour earlier, showing clear dispersion but with lower intensity. More detailed discussion of these points, using GEOS-II data as well as further discussions of SCATHA data, will be given below.

The ion data from the GEOS-II satellite [Korth et al., 1978] to be used in this study consist of detailed intensity plots of fluxes at several pitch-angle and energy channels obtained during the data interval. Figure 5 shows a survey plot of fluxes in the 8:00-13:00 UT interval at two pitch angles: (a) $85 - 95^\circ$ and (b) $145 - 155^\circ$. It is seen that there are small instantaneous plasma responses to the sudden commencement at $\sim 8:30$ UT and to the IMF southward-turning shortly after 10:00 UT, although these are not the main signals affecting the entire spectrum of plasma energies. This is clearly seen by comparing GEOS-II data with SCATHA data on Figure 4. The low-energy instantaneous signals of Figure 5 may be due to magnetic changes [e.g., Baker et al., 1985]. The delayed convection responses to be studied are found in the 11:00-12:00 UT interval. The curious features of this response are that a dispersive response signal is seen at all energies between 27 keV and 225 keV for non-perpendicular fluxes and that a basically dispersionless signal is seen at channels below ~ 75 keV for perpendicular fluxes [Korth et al., 1983; Korth et al., 1984]. In every energy channel, the non-perpendicular flux increases clearly arrive earlier than the perpendicular fluxes, similar to the formation of field-aligned distributions of electrons in their response to sudden electric field changes [Paper I]. Discussion of this complex response will be amplified further, although it is clear from the response features noted hitherto that a single injection source cannot account for them all. This is not to say that the injection boundary model needs to be abandoned; rather, the data convey the need to sort out the sources of the plasma components and to determine how they are transported from these diverse sources at the initiation of an injection event, which may or may not be appropriate for application of the injection boundary model.

A key to clarifying the complex response signal to the above time-dependent changes of the magnetospheric electric field is data from SCATHA. We shall use both the Lockheed mass spectrometer and Aerospace electrostatic analyzer data in this study. As survey of the event, the Lockheed mass spectrometer data is shown in

GEOS-2

22 MARCH 1979

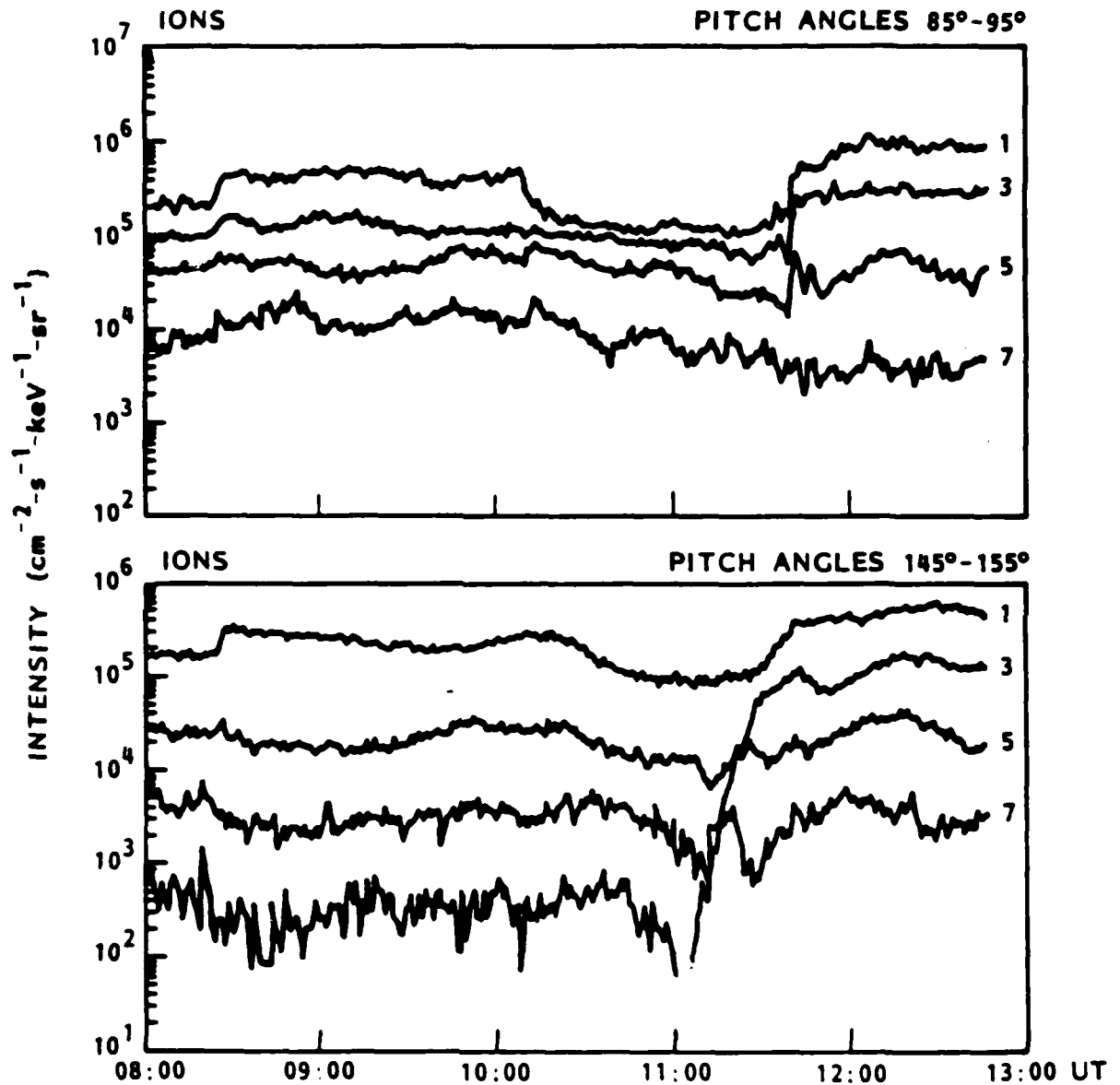


Figure 5. Ion Flux Intensities Measured by the MPAE GEOS-II Instrument in the Data Interval for Two Pitch Angles Highlighting the Two Distinct Dispersion Features. The ion energy channels are: (1) 27-35 keV, (3) 45-59 keV, (5) 75-98 keV, and (7) 129-169 keV.

Figure 6 [Strangeway and Johnson, 1983]. This figure shows the noted dispersion feature after 12:00 UT which was attributed to the injection boundary hypothesis for both hydrogen and oxygen. Two features which are crucial in untangling the curious signals of GEOS-II are not shown in this figure. One of these is the low-energy population mentioned in Figure 4 above, although the high-energy portion is faintly visible in Figure 6 also. Secondly, since the GEOS-II ion data, briefly discussed above, shows the pitch-angle-energy dispersion noted in electron responses in Paper I, one is tempted to ask if the composition of the two ion sources characterized by different dispersions may also be different. Composition, energy and pitch-angle relationships may perhaps help us resolve the two dispersion features shown in the GEOS-II data. Prompted by such theoretical notions, we attempted to sort out the mass-pitch-angle relationship with mass spectrometer and electrostatic analyzer data, which will be discussed in detail in Section V. Identification of two distinct sources of ions for the inner magnetospheric equatorial region has been made [e.g. Fennell et al., 1981; Quinn and Johnson, 1985]; however, our attempt here is not only to identify but to trace their origins as well.

The advantageous upstream location of ISEE-I during this data period has the potential to resolve the mysterious appearance in the inner magnetosphere of two ion populations with distinctly different dispersion signatures. Noting that the global time-dependent electric field model is in approximate agreement with the plasma flow data on ISEE-I, at least before 12:00 UT, we next considered the ISEE-I mass spectrometer data. Figure 7 shows that the ISEE-I Lockheed instrument response is a disappearance of hydrogen (reduction of total ion density) coincident with the start of an increase in oxygen, both occurring at the ~11:10-11:30 UT interval—earlier than the responses downstream. Further, intensity-spectra of both components at different pitch angles during this period, such as that shown on Figure 8, indicate that they are basically isotropic. The reduction of hydrogen and enhancement of oxygen upstream together with the occurrence of two distinct dispersion features downstream are factors that will play a major role in our interpretation of the injection event.

The above is a summary survey of the ion data that are included in the study. They are presented in a logical sequence with accompanying references to the underlying theoretical reasoning leading to their selection, although a coherent interpretation is not intended in this section. In the following sections, this data framework will be amplified with details.

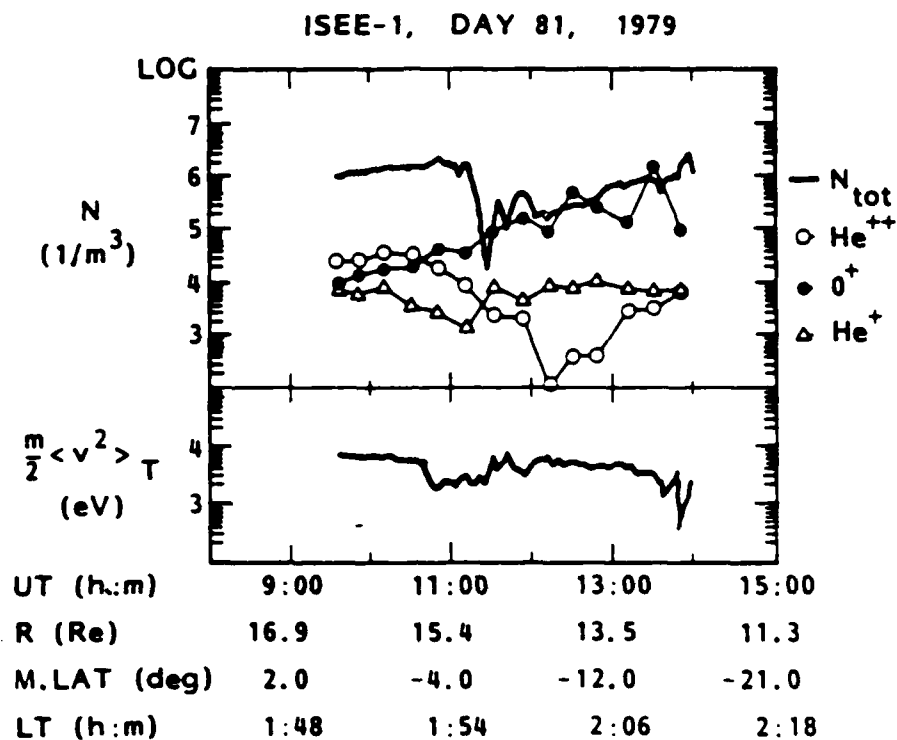


Figure 7. Ion Number Densities (Top Panel) Measured by the Lockheed Mass Spectrometer on ISEE-1 (0.1-16 keV/q). The solid curve without symbols is based on the total ion flux through the electrostatic analyzer section of the instrument and assumes that this flux is dominated by H^+ . The temporal resolution of this curve is about 2 minutes, whereas the resolution of the labeled curves (determined by the mass analyzer) is about 20 minutes. The bottom panel indicates the thermal energy of the ions, also determined by the electrostatic analyzer.

ISEE-1, DAY 81, 1979, 11:25 UT-11:54 UT

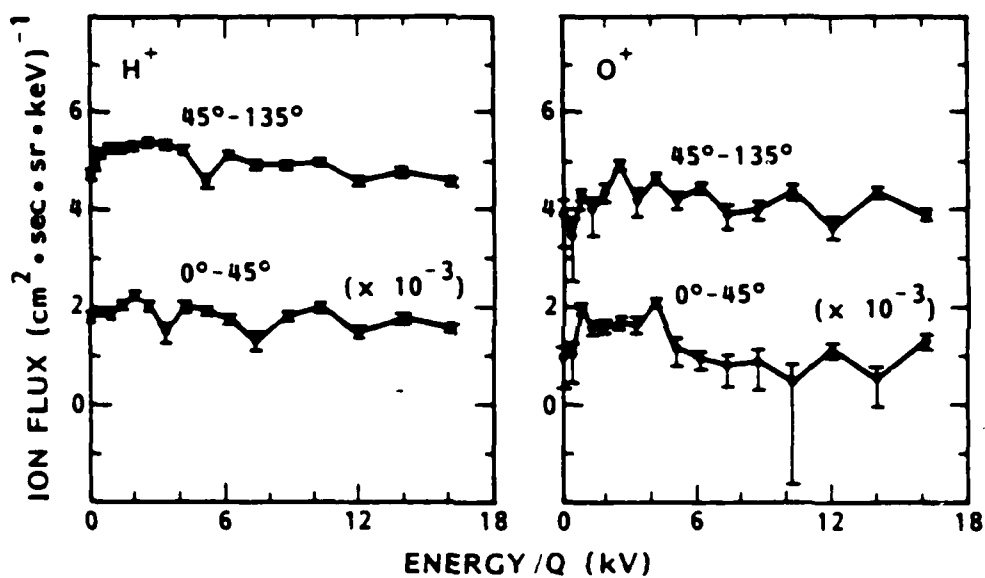


Figure 8. Hydrogen and Oxygen Energy Spectra Measured for Two Pitch Angles by the Lockheed Instrument on ISEE-1

IV. THEORETICAL FRAMEWORK

In Paper I, the emphasis is on modeling changes of electron distributions in response to time changes of the electric field. Here, the goal is really the same except that we are dealing with a much larger data base which has not been completely reduced into distribution function form. Further, the *modus operandi* here is to map ion distributions backward in time from observation points to find out where they would have been if the global electric field model was operational; whereas, in Paper I, electron distributions were mapped forward in time from assumed sources and electric fields which were not constrained by observations. Because observational constraints are much tighter here and because the data have not been reduced to distribution form, we shall proceed with the study by mapping representative ions with various energies and pitch angles instead of attempting to construct entire distribution functions. We shall, however, invoke the characteristic responses of distributions discussed in Paper I when necessary.

An important complication in the interpretation of inner magnetospheric ion responses is that both hydrogen and oxygen can be major components but their sources, and thus convection responses, are different. However, this complication is to be distinguished from adiabatic transport which depends on energy/charge and not on mass *per se*. Trajectories for ions of equal charge and different masses are the same if their initial pitch angle and magnetic moment are the same. This means that we need only show hydrogen trajectories. Oxygen and hydrogen trajectories for a given initial pitch angle are the same if the oxygen initial energy is the same as that of the hydrogen. Multiply charged ions will not be considered in this study, hence the word "ion" will be used to denote proton unless specifically noted otherwise.

In order to present the theoretical results systematically, trajectory traces are organized into three groups according to initial ion energies at the observation points: (A) low energy ions of 10-500 eV, (B) intermediate energy ions of 1-60 keV, (C) higher energy ions of 80-150 keV. These groups of trajectory traces are represented in Figures 9 to 13 by showing traces at a few specific representative energies in order to reduce clutter. Figure 9 shows trajectory traces from GEOS-II (G) and SCATHA (S) for the low energy group represented by 10 eV ions. Figures 10 to 13 show trajectory traces of the intermediate and high energy groups, represented by 1, 10, 110, or 150 keV ions

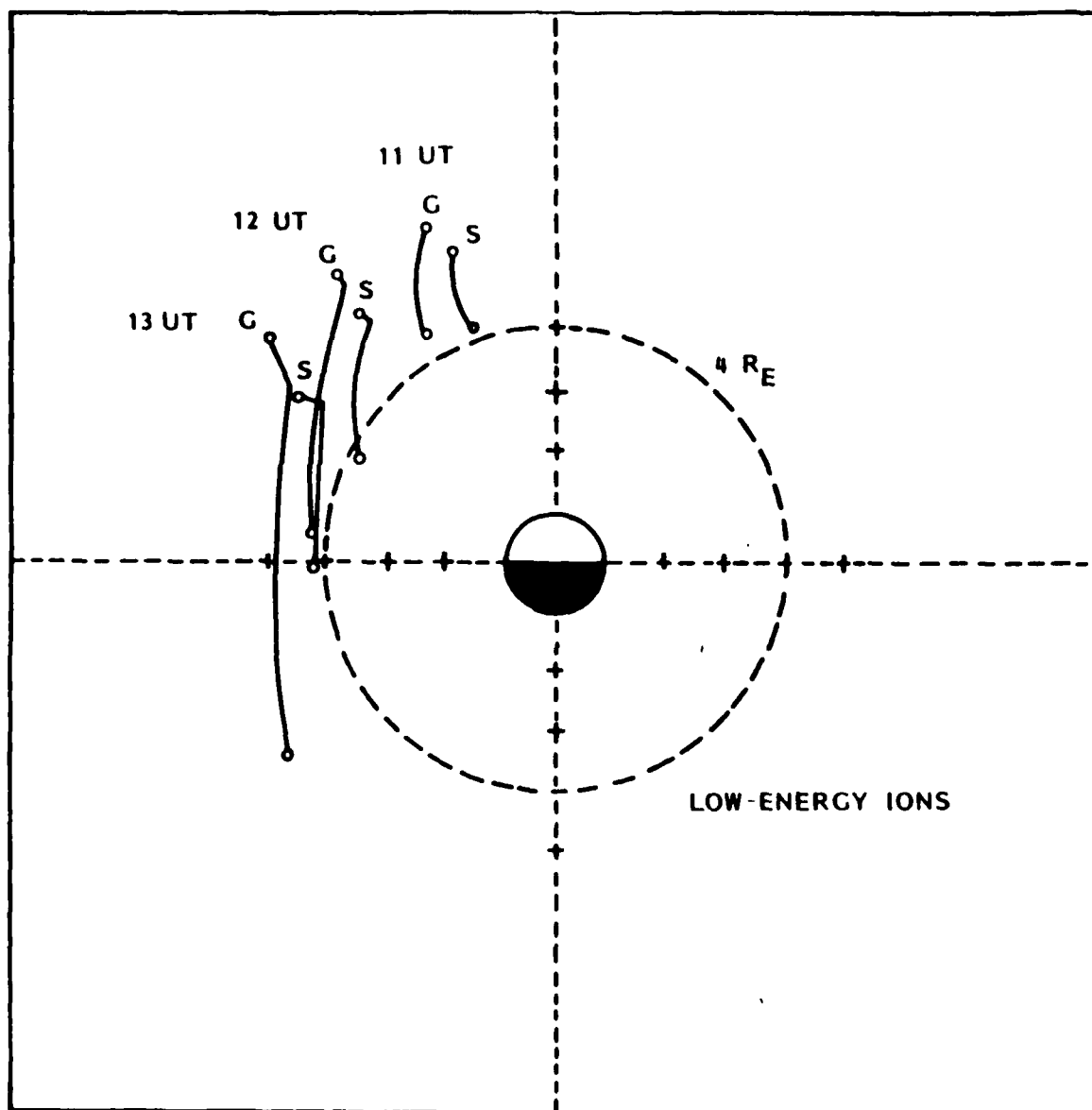


Figure 9. Backward Trajectory Traces with Our Convection Potential Model from SCATHA (S) and GEOS-II (G) for Low Energy Ions Represented by Those of 10 eV Initial Energy and 90° Pitch Angle

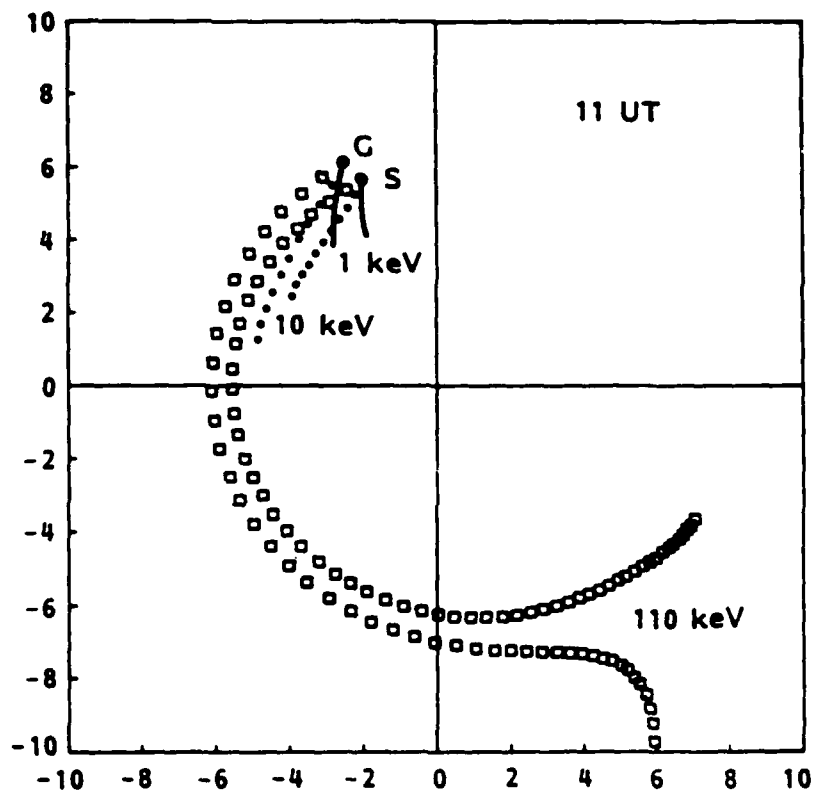


Figure 10. Backward Trajectory Traces with Our Convection Potential Model from SCATHA (S) and GEOS-II (G) for Intermediate and High Energy Ions at 90° Pitch Angle and Starting at 11:00 UT

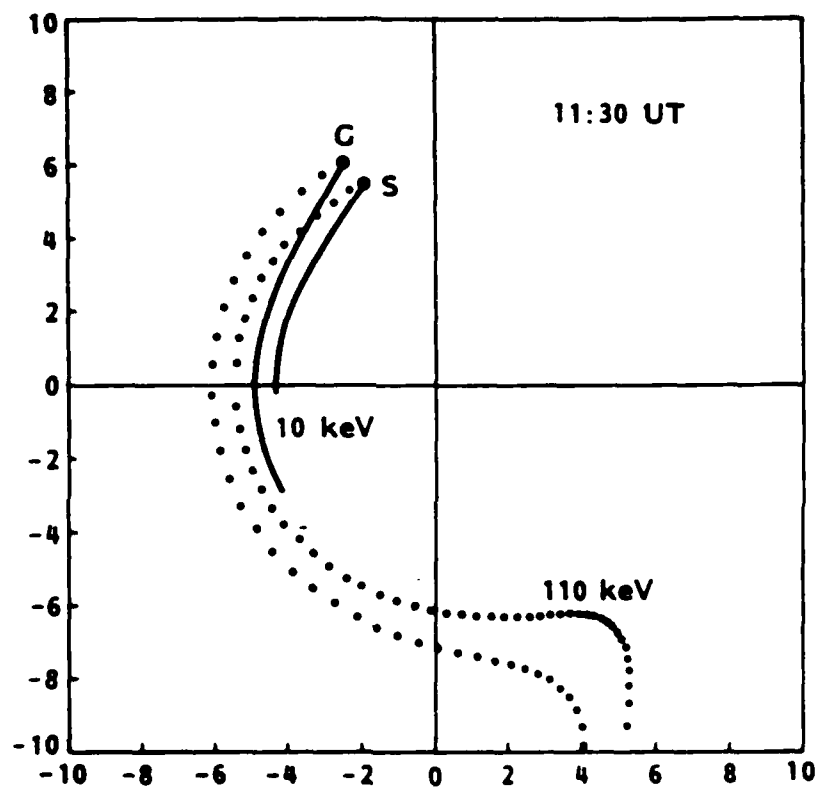


Figure 11. Same as Figure 10 but for Backward Tracing from 11:30 UT

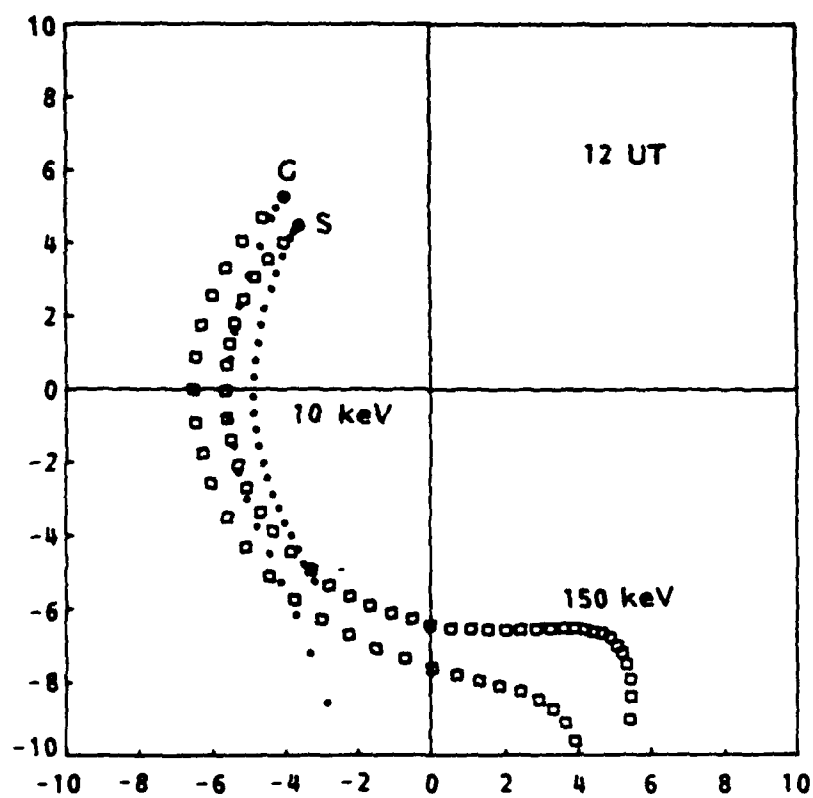


Figure 12. Same as Figure 10 but for Backward Tracing from 12:00 UT

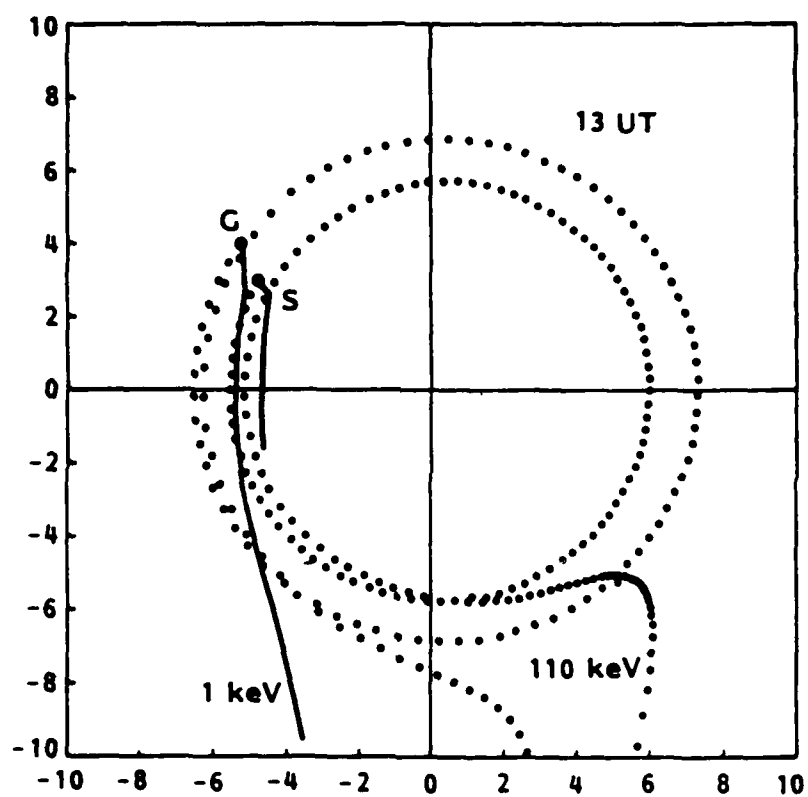


Figure 13. Same as Figure 10 but for Backward Tracing from 13:00 UT

when appropriate, at 11, 11:30, 12, and 13 UT respectively. The trajectory traces in Figures 9 to 13 start backwards from the specified time and location to one time step earlier than the southward turning of the IMF at 10:08 UT. Time steps for low-energy ions are not shown, but for intermediate and high energy ions in Figures 10 to 13, each time step, represented by the interval between markings appropriate to the particular ion trajectory, is 0.038 hr. for Group B and 0.015 hr. for Group C trajectories. Trajectory tracing outside of the $10 R_E$ by $10 R_E$ box is not shown. Since the time resolution of mass spectrometers is approximately twenty minutes, no attempt has been made to do timing studies between ISEE-I and the two inner-magnetospheric satellites, other than the rough temporal relationships noted in the previous section. Without ion distribution function data of sufficient time resolution at ISEE-I, it would be futile to do a quantitative mapping to identify the two source distributions. It was emphasized in Paper I that pitch-angle distributions of populations arriving at a given time and location are most distorted at those energies which brought the ion trajectory near a stagnation orbit some time in the past; however, without distribution function measurements with high time-resolution upstream, we are unable to exploit this feature. Consequently, only 90° pitch angle traces are presented here. Traces for 30° pitch angle have been made, but no significant differences, other than those noted in Paper I, were found to affect our results here.

Particular features that bear on the interpretation of data will be discussed in Section V; however, it may be of interest to note the general features of the complex temporal-spatial-energy relationships here. Comparison of the corresponding energy traces in Figures 10 to 12 shows the obvious feature that the two jumps in the electric field strength, at 10:08 UT and at 11:40 UT, have profound effects upon the question of sources of ions arriving at the inner-magnetospheric satellites. Ions below 1 keV do not map to the tail until well after 13:00 UT, in general agreement with Strangeway and Johnson [1983], though not shown here. But the interesting feature is that these low energy ions map inwards towards the plasmasphere. Group B (intermediate energy) ions do not map to the tail until after 11:30 UT, and there is little evidence of trajectories coming near stagnation orbits except at late times. Group C (higher energy) ion orbits undergo profound changes at various times. Before 11:30 UT, the stagnation orbits for this group are clearly between SCATHA and GEOS-II orbits. By 12:00 UT, however, both satellites are accessible to these ions from the tail, but

by 13:00 UT the general initial situation pertains again. This is very important for exploring the question of what constitutes the injection boundary—a subject to be considered in the next section. Meanwhile, it is very important to point out that, if one examines the trajectories for the entire range of observed ion energies under the action of a tested global electric field model, the sources of ions certainly cannot be limited to a particular location or boundary during the data interval, which is the initial phase of a substorms injection event. This is not to say that no boundary sources can be present because trajectory tracing has nothing to say about the presence of plasma prior to or outside of the space-time interval considered. Rather, we take the view here that we are observing the formative stages of a boundary source during our data interval.

V. DISCUSSION AND INTERPRETATION

In this section, specific features of observations and theory will be brought into contact with each other, to be followed by a synthesis of the various pieces of evidence into a possible, perhaps even plausible, view of the meaning of an injection in the inner magnetosphere.

(A) Source of low energy ions.

It was pointed out in Section III and Figure 4 that a population of low-energy ions (< 1 keV) arrived at SCATHA at about 12:00 UT and disappeared just after 13:00 UT, well before the low-energy portion of the "injection" was encountered. What is the source of this low energy population and what does it imply about the transport processes in the inner magnetosphere? From Figure 9 it is seen that such ions map inwards from inside SCATHA orbit. The source of this population can be pinpointed if the model electric field is taken seriously because the trajectories mapped from 11:00 UT and 12:00 UT end at very different local times and radial distances: the 11:00 UT trajectory maps to $5 R_E$ at 1:00 PM and the 12:00 UT trajectory maps to $4 R_E$ at 6:00 PM, as does the 1 keV trajectory from 12:00 UT. The locations of the trajectory end points indicate that there must be a source of very low energy ions at the plasmaspheric cloak region at the local time of the plasmaspheric bulge at the time of the southward turning of the IMF. The trajectory tracing clearly connects the observed population with the low-energy population previously described by Olsen [1981]. Since outward convection decreases particle energy, these ions are likely to have acquired their warm temperatures through wave-particle interaction at the outer plasmasphere prior to outward convection [Young et al., 1981; Roux et al., 1982]. If so, we would expect a source of warm ions convecting outward to SCATHA, thus accounting for the absence of > 1 keV ions in the data.

The plasmaspheric bulge and cloak are fairly constant features of the inner magnetosphere; thus we can say, *ex post facto*, that it would be surprising if we did not find this "unexpected" low energy population at SCATHA since the electric field model is a reasonable approximation to reality, and SCATHA is at the right location to intercept the ions drawn from the plasmaspheric cloak. Further, if our theoretical interpretation is correct, this equatorially trapped population must contain a high proportion of ions with perpendicular pitch angles [Roux et al., 1982]. The Lockheed

mass spectrometer on SCATHA observed the high-energy tail of this population at 100-600 eV, and it shows that the hydrogen population is mainly perpendicular [J. Quinn, personal communication]. From a different point of view, the appearance of this intense population is clear evidence that during an injection event the action of a temporal jump in the convection electric field cannot be denied. This is not to say that the low energy population is convected outwards to SCATHA by action of the electric field jumps only; the emphasis here is that timing of the jump and location of the source virtually exclude other possibilities. Since the electric field acts on all plasma, its effect upon the ions in the inner plasmashet cannot consequently be denied, thus leading to the next logical step of determining the characteristics of the hot ion response to the observed jump in the electric field.

(B) Dispersion of Intermediate and High Energy Ions.

In the preliminary discussion of the GEOS-II data in Figure 5, it was noted that there was a clear difference of dispersion between the perpendicular and off-perpendicular ions. This is an important feature since ions marking dispersion features at the initial stages will properly be traced back to the initial location of the source of injection, whereas those arriving later may do so because either they were injected later or because they have lower energy. Not knowing the temporal behavior of the source, the initial ions in a given energy channel and their dispersion yield the most important information on their source locations. The crucial question here is whether the two different dispersion features mark two different populations from two different sources or are the two dispersion features resulting from an interplay between pitch angle and energy of a single population. The reason why this is a crucial question is simply that if there are multiple sources of keV ions which do not exhibit the same dispersion, then the "injection boundary" cannot be a single boundary with a single dispersion signature, at least in the initial phase of its formation or evolution. The mechanism of its evolution into a single boundary is then its mechanism of formation.

In order to answer this key question, we examine six separate facets of the problem with both data and theory. Some of the factors studied here may bear general relationships with other studies which are more concerned with substorm injection than with the detailed nature of injection boundary formation [e.g., McPherron and Manka, 1985; Stokholm et al., 1985]. The particular features under investigation here are: (i) examine GEOS-II ion data with finer resolution over a spectrum of pitch

angles to see if there are really two dispersion features or if Figure 5 shows an optical illusion, (ii) examine GEOS-II electron data to see if there are two dispersion features indicating two electron sources associated with the two possible ion sources, (iii) examine high resolution SCATHA ion data to see if similar two-component dispersion features are also seen, (iv) examine SCATHA ion mass spectrometer data with as much time resolution as possible to see if the dispersion features may be related to mass components, which may allow for source identification, (v) examine ISEE-I ion data to determine if features observed downstream can be traced to specific features observed upstream at ISEE-I orbit, and (vi) examine theoretical ion trajectories mapped with the tested global electric field model to see if a consistent synthesis of the observed dispersion of intermediate and high-energy ions can be made. The detailed discussions below will lead to the conclusion that there is more than one ion source, and clearly more than one dispersion feature in an event which, when seen with low resolution data and at later times (after 14:00 UT), appears to have a single dispersion.

(i) GEOS-II Ion Dispersion:

Figure 14 shows a panel of four ion intensity measurements covering four pitch-angle bins and several energy channels. These figures, together with the two similar panels of Figure 5, cover the entire range of pitch angles. It is clearly seen that the dominant dispersion feature, covering the entire energy range of 27-225 keV, started at about 11:10 UT, also covered the entire pitch-angle range. A second dispersion feature appears in the three pitch-angle panels surrounding 90° and is prominent only in the lower energy channels below ~ 100 keV. Further, the second dispersion feature, starting at about 11:40 UT, is clearly distinguished from the first feature on the channels on either side of 90° pitch angle, showing almost no energy time dispersion. Since the two features differ on all measured characteristics attributed to adiabatic dispersion and are seen to exist as separate and distinct features on the same pitch-angle bins, we have no choice but to assign to them separate identity. There are two very important non-dispersive points about the two features: (a) they seemed to have "merged" at the lower energy channels just before 12:00 UT at GEOS-II so that after 12:00 UT no dispersion feature is identifiable, (b) before the merger the two features were clearly pulses of increased flux and not step flux increases characteristic of a source boundary. Without lower energy data, it is difficult to say whether a true

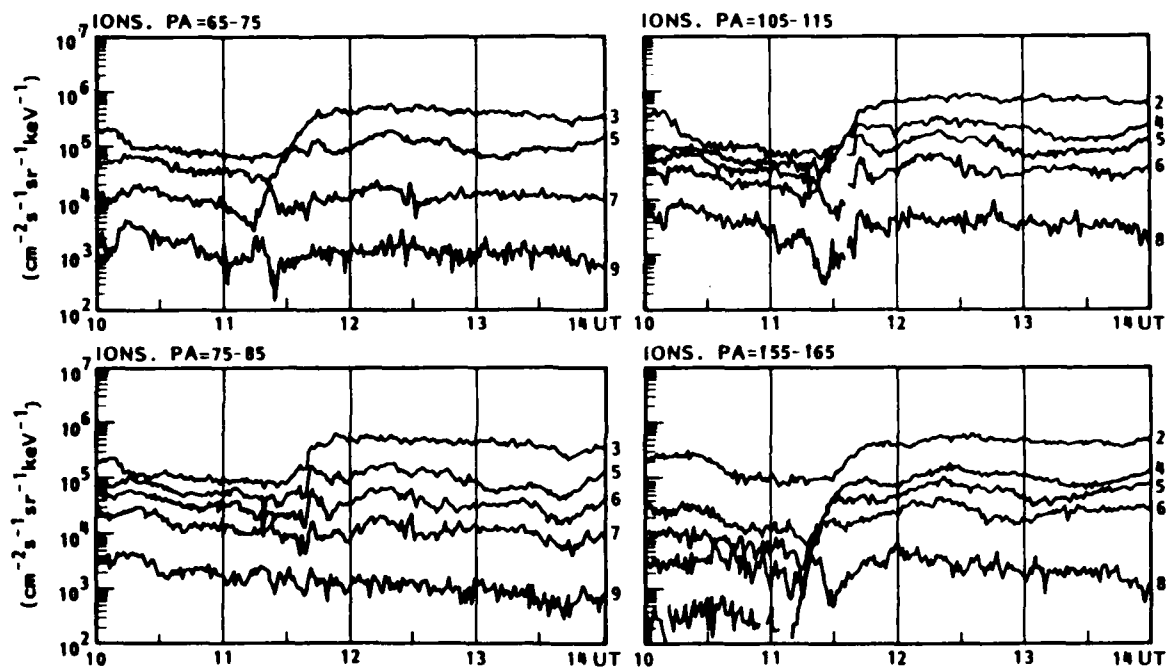


Figure 14. Same as Figure 5 but for the Remainder of the Complete Set of Pitch Angles. The ion energy channels are: (2) 28-36 keV, (3) 36-45 keV, (4) 45-59 keV, (5) 59-75 keV, (6) 75-98 keV, (7) 98-130 keV, (8) 130-169 keV, and (9) 169-226 keV.

merger took place or that the two features just happened to cross each other at the low energy threshold of the instrument (27-35 keV) at the same time, but characteristics of a single source boundary seems to be consistent with this merger.

(ii) GEOS-II Electron Dispersion:

Although electrons of keV energies follow very different convection paths, resulting in very different arrival times, electron dispersion signatures are still relevant in determining whether one or two populations were present and whether the crucial "merger" of ion features noted above is accidental or not. Figure 15 shows a sample of electron fluxes measured at GEOS-II. Two dispersion features are clearly identified. The features "merged" at about 12:20 UT. The similarity between the mergers in both ion and electron data favors the view that the merger is real and not simply a coincidence, for it would be rather unlikely that the two dispersion features just happen to cross each other exactly at the lowest channel of the instrument for both ions and electrons.

(iii) SCATHA Pitch-Angle Data:

Figures 16 and 17 show a summary of the SCATHA SC-2 ion measurements during the crucial period before 12:00 UT. In Figure 16, it is seen that the responses in energy channels below ~ 100 keV are quite complex. Above ~ 100 keV, small pitch angle fluxes show small rises and 90° pitch angle fluxes show small drops simultaneously. But, these intensity changes are much smaller than that of the lower energy channels. For the lowest energy channel, a gradual rise of both perpendicular and parallel fluxes started at about 11:40 UT culminating in a sudden increase in the perpendicular flux at 12:00 UT which was confirmed by the next two higher energy channels. The detailed development of the pitch-angle distribution, summarized in Figure 17, is quite complex before 12:00 UT. It shows a perpendicular minimum propagating in the lower energy channels from high to low energy until 12:00 UT, when a perpendicular population arrives to fill in the deficiency thus ending up with a pitch-angle distribution almost the same as the initial one. The flux rise after 11:40 UT and the arrival of a perpendicular population later are reminiscent of features in the GEOS-II data, although several differences need to be amplified before a consistent interpretation can be made.

GEOS-2 22.03.1979
ELECTRONS, PA=85-95

EXP. S321/MPAE
11 EMF AVER

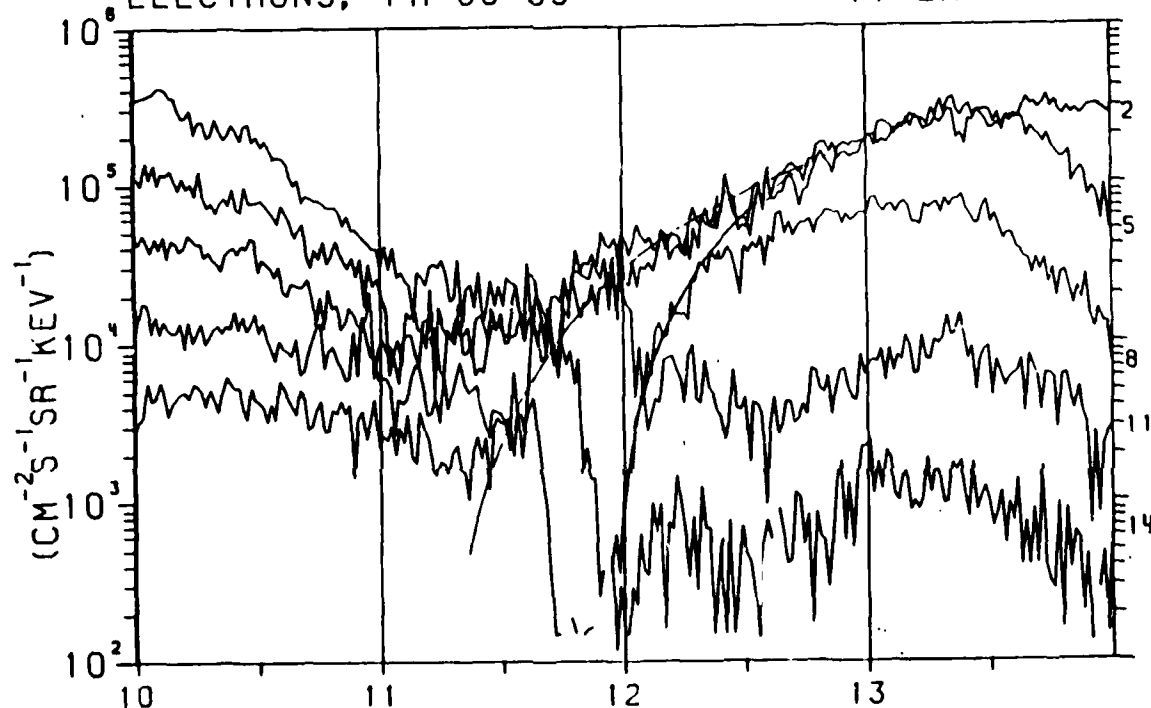


Figure 15. Electron Flux Intensities Measured by the MPAE Instrument on GEOS-II Exhibiting Two Distinct Dispersion Features Which "Merged" at a Later Time, but Within our Data Interval. The electron channels are: (2) 24-30 keV, (5) 45-52 keV, (8) 71-83 keV, (11) 114-133 keV, and (14) 180-214 keV.

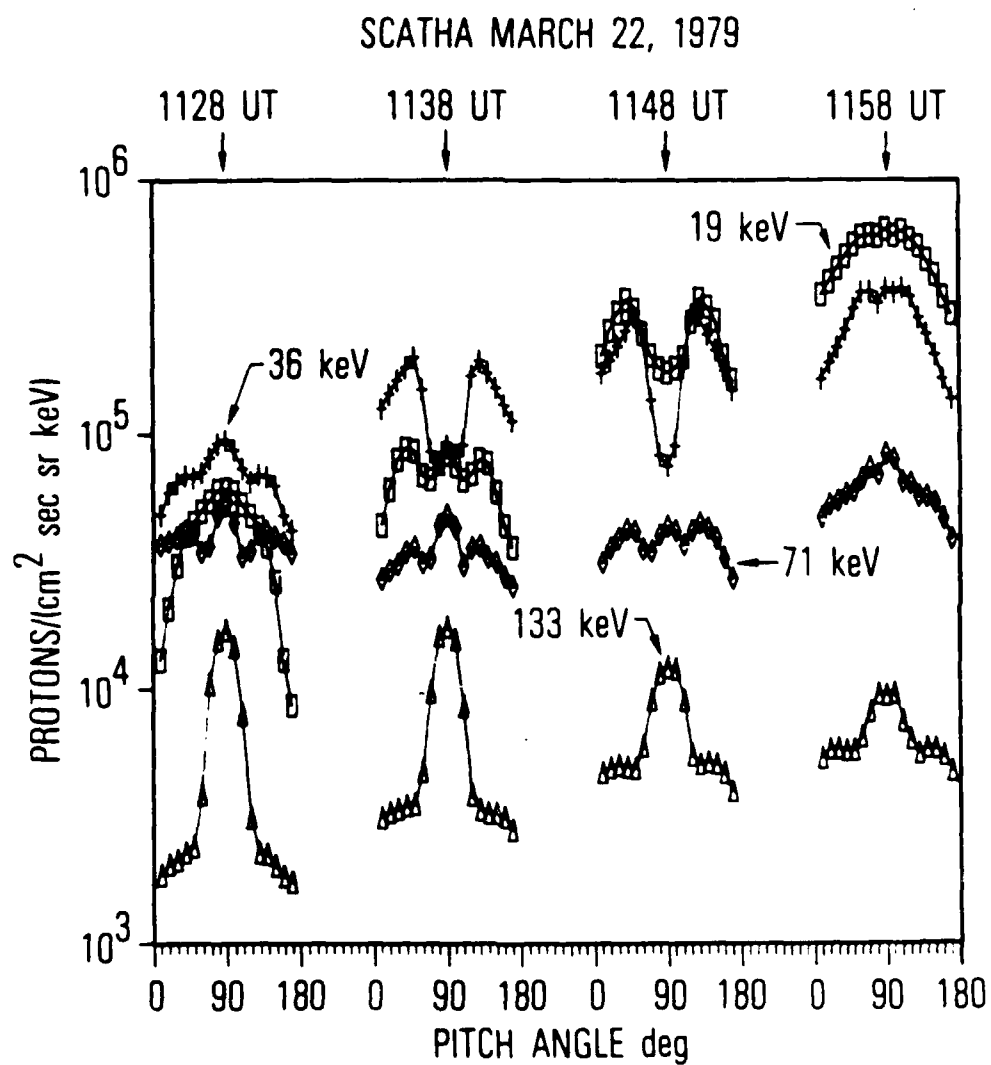


Figure 16. Temporal Development of Ion Pitch Angle Distributions Measured by the Aerospace Instrument on SCATHA

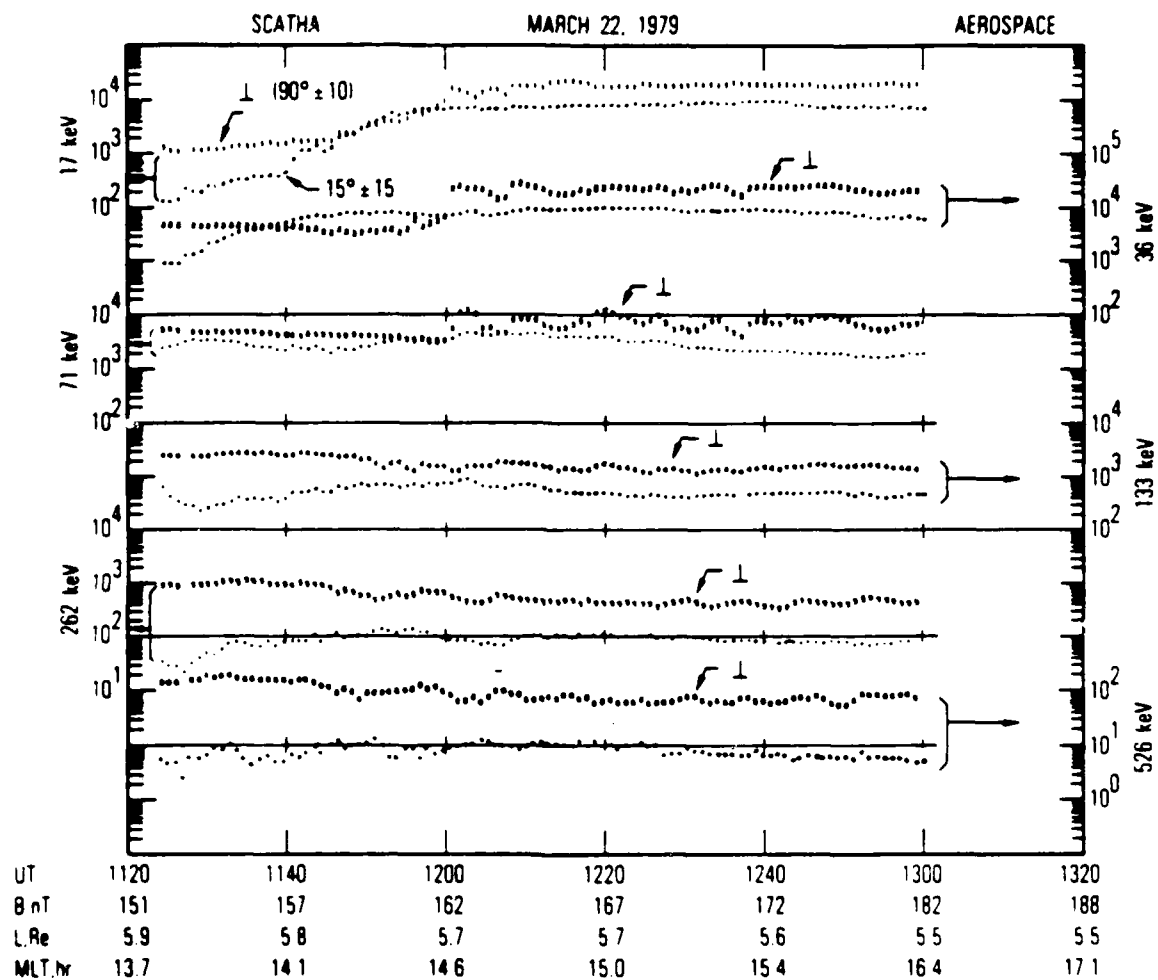


Figure 17. Flux Intensities of Ions at $90^\circ \pm 10^\circ$ and $0^\circ - 30^\circ$ Pitch Angle Measured by the Aerospace Instrument. The former is indicated by the trace of energy channel numbers and the latter is indicated by the associated trace of dots.

First of all, the pitch-angle distribution of the main dispersion feature in Figure 14 is isotropic, whereas the dispersion feature before 12:00 UT discussed above shows complex changes in the pitch-angle distribution. From Figure 17, the changes are apparently a developing deficiency in the perpendicular flux as discussed above, rather than a flux increase at intermediate pitch angles. Second, from Figure 16 it is apparent that the response starting at 11:40 UT is limited to below 54 keV, and the response of perpendicular ions at 12:00 UT is limited to below 104 keV; whereas, from Figure 14 the main dispersion feature covers the entire spectrum of the instrument, and the perpendicular ion response is limited to below ~ 100 keV.

(iv) SCATHA Ion Mass Spectrometer Data:

From the discussions above, the Aerospace plasma data are consistent with arrival of two populations of ions which merged after 12:00 UT to yield the single dispersion feature invoked by Strangeway and Johnson [1983] as signature of an injection boundary. If two populations coalesce into a single feature that shows the characteristics of the injection boundary, then the mechanism of the merger is simply the physical process which forms the "injection boundary." Quinn and Johnson [1985] showed that oxygen and hydrogen behaved differently in the injection region; therefore, it is of interest to investigate the mass composition of features identified by pitch-angle behavior. Figure 18 shows pitch-angle properties of oxygen and hydrogen measured by the Lockheed ion mass spectrometer on SCATHA during the data interval. Because of poor counting statistics, long averaging durations are required to obtain meaningful pitch-angle data; therefore, the complex pitch angle changes prior to 12:00 UT are not apparent in this data. However, comparing intensity levels, the data show clearly that the increase at 12:00 UT of perpendicular ions in the keV range is mainly hydrogen at channels above 10 keV.

(v) ISEE-I Mass Spectrometer Data:

Is the perpendicular hydrogen population which appeared at 12:00 UT at SCATHA and, by inference based on pitch angle features, appeared at 11:40 UT at GEOS-II, the same hydrogen population which disappeared at ISEE-I orbit? Observations of suprathermal ions at ISEE-I orbit have been reported [Ipavich et al., 1985]; however, it is the thermal population that is relevant here. The Lockheed ISEE-I mass spectrometer response is shown on Figure 7, which indicates that at

SCATHA IONS - DAY 81 1979

$\Delta = H^+$

$\bullet = O^+$

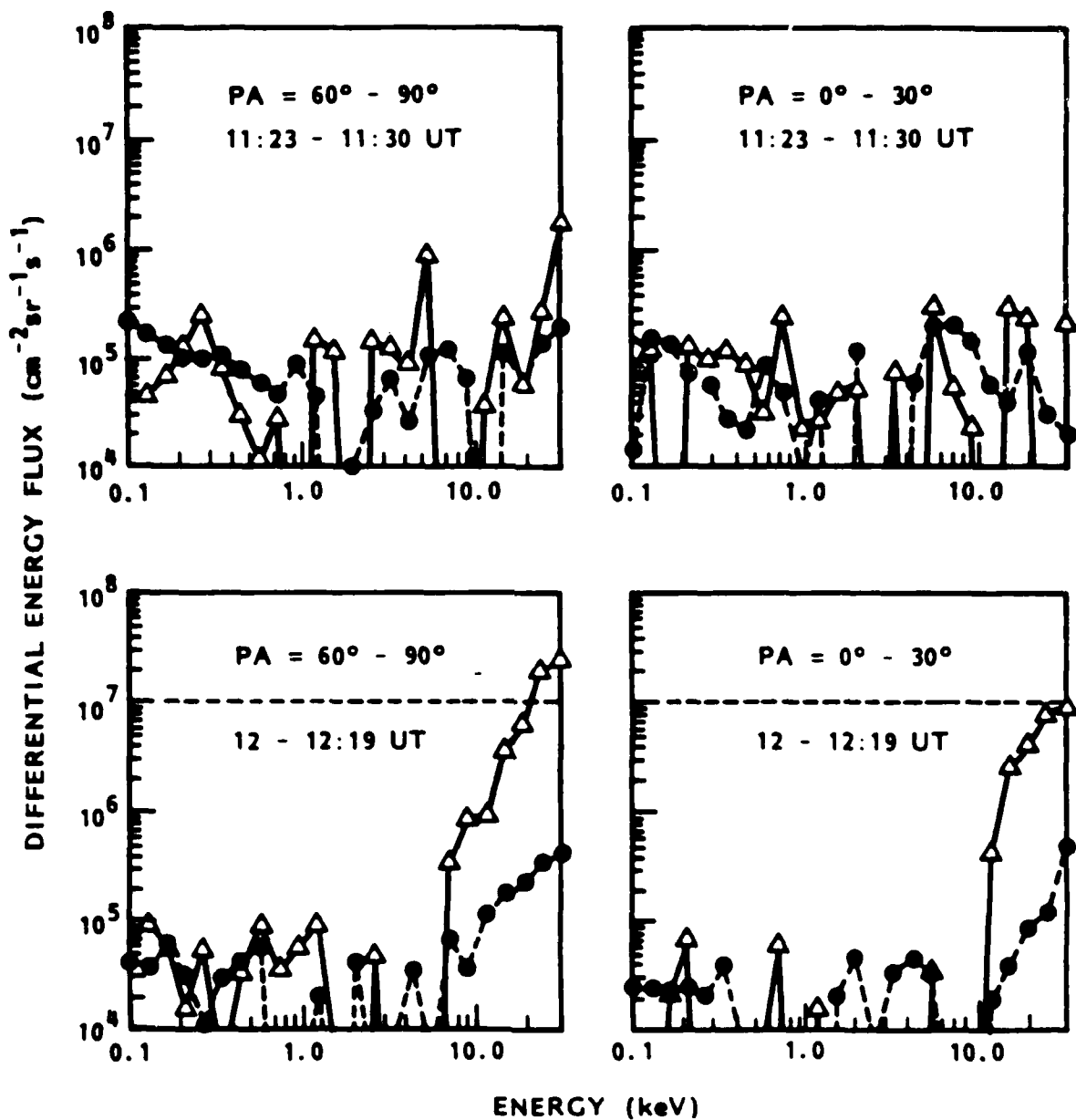


Figure 18. Temporal Development of Flux Intensities of Hydrogen and Oxygen Measured by the Lockheed Mass Spectrometer on SCATHA for Two Pitch Angle Bins. Averaging time for each panel is ~ 20 minutes.

11:10-11:30 UT a simultaneous decrease of hydrogen and increase of oxygen occurred. Further, the decrease in hydrogen actually signifies a decrease of solar wind plasma because He^{++} is seen to decrease also. Since the plasma flow at ISEE-I is generally sunward, as indicated both by observation and theory, the hydrogen signature at SCATHA and GEOS-II can be accounted for by assuming an ISEE-I encounter with a region where hydrogen has gone sunward at an earlier time. However, the oxygen increase, whose origin can only be high-latitude auroral activity, would argue that auroral activity increased almost simultaneously and that oxygen arrived from the auroral zone to fill the void. Both components are still continuing the inward flow at the time of encounter. This simple postulate takes into account all the observed features naturally without additional postulates. Since electric field changes from 10:00 UT onwards have been included in the model and no magnetospheric changes have been reported since the old sudden commencement at $\sim 8:25$ UT, additional complex postulates would be required for alternate interpretations. For our interpretation of what constitutes the formation stage of an injection, we adopt this simple hypothesis until evidence shows otherwise.

(vi) Theoretical Synthesis:

With the electric field model tested against ISEE-I flow data and interpretation of the low-energy response based on the electric field model tested against SCATHA data, we are now in a good position to synthesize the observed response features at intermediate and high energies into a theoretical interpretation of what constitutes an injection of the keV auroral plasma.

In the data description above, it has been noted that ISEE-I saw its response at 11:10-11:30 UT, perhaps somewhat earlier than the GEOS-II response at > 100 keV; whereas the major SCATHA response at < 30 keV did not start until after 11:40 UT, although very small flux increases are seen prior to 11:40 UT. Inspection of the trajectory mapping in Figures 10 and 11 indicates that the timing is approximately consistent with theory. For example, intermediate energy ions take ~ 15 steps and high energy ions take ~ 35 steps in 30 minutes. Since a dipole magnetic field is assumed, only approximate timing studies are admissible because convection depends on both electric and magnetic fields. Accessibility is, however, the crucial factor which differentiates the structure of the responses. Intermediate energy traces of Figure 10 shows that at 11:00 UT the trajectory end points, which represent the southward

turning of the IMF at 10:08 UT, of both spacecrafts do not map to the plasma sheet where the source is presumably located. By 11:30 UT (Figure 11), GEOS-II is accessible to plasma sheet ions of energy above 30 keV, which is consistent with the main dispersion feature seen by that spacecraft. The access of high energy ions from the plasma sheet at these initial times of the injection is particularly interesting. High energy traces of Figures 10 to 12 show that the stagnation orbit of ~ 100 keV ions at 11:00 UT lies between GEOS-II and SCATHA, moves to just inside of SCATHA orbit at 11:30 UT, and it is not until 12:00 UT before SCATHA is accessible to these ions without undue delay. The effect of this predicted stagnation boundary is consistent with the access of high energy ions to GEOS-II shortly after 11:00 UT and with the cutoff of SCATHA response at these high energies shown in Figure 16. The convection scenario shown on Figure 13 for 13:00 UT is also of interest in that the effects of the IMF northward turning and decrease of electric field magnitude at $\sim 11:40$ UT are now apparent in the inner magnetospheric segments of the trajectories. From Figure 13 it is seen that the stagnation boundary has returned to its old approximate location. Furthermore, the high energy trace of the figure shows that outward motion of the energetic ions, which constitute the stormtime ring current penetrating to $\sim 4 R_E$ in the initial phase of the injection, now add to the population at intermediate energies because of the energy loss associated with outward convection. Unfortunately, there is no way to distinguish such energy-degraded ions from freshly injected intermediate energy ions since this figure also shows that both spacecrafts are accessible to 30 keV ions from the plasma sheet at this time. Based on the work of Paper I, it is clear, however, that such a multiple-source scenario is likely to yield isotropic distribution functions.

With the interpretation of the main dispersion features observed by GEOS-II and SCATHA made fairly consistent with theory based on response to temporal changes of the convection electric field, we have now isolated the known features of the initial dispersion and are ready to discuss the unknown features of the dispersion. The dominant unaccounted for features of all data sets in this study are simultaneous actions connected with component responses: simultaneous increase of oxygen with decrease of solar wind components at ISEE-I orbit and the merger of two GEOS-II dispersion features, one of which is likely to be a perpendicular population rich in hydrogen and identified at SCATHA. These responses are clearly dynamical and are

outside of the scope of the theory of trajectory tracing which has been used above to sharpen our focus on the dynamics. Based on the agreement between observed and predicted flow patterns at ISEE-I orbit, we hypothesized that a population of solar wind plasma has been transported inward shortly prior to the auroral activity which injected oxygen into the cavity left behind. The inward-transported solar wind plasma is later encountered by both GEOS-II and SCATHA as the perpendicular population of hydrogen ions. This solar wind population of ions and the associated electrons constitute the second dispersion feature, which is primarily of intermediate energy, indicating their origin as plasma remnant from quiet times. Meanwhile, the injected auroral plasma, containing high proportions of oxygen ions, formed a separate but distinct pulse feature which moved inward to GEOS-II orbit, where it appears as the first dispersion feature. The associated electrons of these two plasma pulses also propagate inward and were encountered as separate but distinct dispersion features. The observation of inward propagating plasma pulses has been reported previously [e.g., Moore et al., 1981]. The observation of two separate but distinct convecting pulses in this study is novel but not entirely out of the realm of expectation. The "main event" of the inner magnetospheric ion response, however, is the merger of the two dispersion features which occurred at 11:40 UT at GEOS-II and at 12:00 UT at SCATHA, indicating inward propagation of a "merged" plasma. If our reconstruction of the plasma convection scenario is correct, this merger of two plasmas is significant in that (a) prior to the merger the two dispersion features were pulses, but after the merger the dispersion response at low energies showed the characteristic step structure of an injection boundary, and (b) it took place in the inner magnetosphere as both SCATHA and GEOS-II encountered the high energy components in pulse form prior to the merger. According to Strangeway and Johnson [1983], the inward propagation of what we would refer to as "merged plasma," as deduced from the location of SCATHA from 12:00 UT onwards, fits expectations of the *ad hoc* injection boundary model. Not being official members of the injection boundary community, we have no way to determine whether the event studied here qualifies for the injection boundary model or not; however, a merger of two dispersion features did take place, and the characteristics of the plasma in terms of flux and pitch-angle distribution are different after the merger which later involves electrons as well. We are thus tempted to identify this merger of two plasmas, old solar wind plasma and new plasma of

auroral origin, as formation of the injection boundary. This new hypothesis seems to fit our observations, thus it is perhaps worthwhile to see where it may lead us. In this regard, comparison of the merger of electron dispersion features will be significant. This item will be the topic of our next investigation. It should be noted that the exact location and shape of the *ad hoc* injection boundary are not yet of concern since these are statistical constructs [e.g., Mauk and Meng, 1983].

What would we expect from the kinetic theory of auroral plasma formation if the merger of two plasmas took place according to the scenario as synthesized by our theoretical considerations of trajectory tracing? The crucial kinetic theoretic element in the above scenario is that the merger may be the result of one plasma overtaking another. The overtaking need not be confined to motion in the equatorial plane since the auroral ions are perhaps more likely to stream into the solar wind ions along a direction which is the result of their field-aligned and convection motions. We have investigated the ISEE-I plasma flow vector in detail, and this seemed to be the case. However complex the scenario of overtaking, if differential velocities and densities meet strong two-stream instability criteria, wave-particle interaction can produce sufficient turbulence to isotropize the resultant plasma so that it acts as a new plasma—a main ingredient ascribed to the plasma characteristics of the *ad hoc* injection boundary. In order to form a new plasma at a boundary across which there is no “memory” of its component past, strong turbulence generation is required in the merger. Theoretical modeling of the scenario suggested here will be treated as a separate paper of this series. Meanwhile, we hope to have introduced a new element into consideration of plasma injection in equatorial regions, namely the importance of the temporal behavior of the source and, consequently, the component dispersion behavior, because those dispersion features that do not meet instability criteria to merge will pass through each other retaining their separate identities. Apparently, such features have been noted and attributed to the *ad hoc* injection boundary hypothesis. If the scenario suggested here is verified, a fundamental change in our view of auroral activity will be implied since the auroral process will be seen as active at the initiation of substorm injection and not as a final sink in a temporal chain starting with storage and magnetic merging. Correlation of auroral imagery with timing of IMF changes may have already initiated this trend of thinking about the auroral process [Frank, 1985] since auroral activation seems to be contemporaneous with IMF changes. In

our case this scenario is suggested by the simultaneous decrease of solar wind ions and increase of oxygen in our ISEE-I observations. A second element in the scenario we have constructed that may also be noteworthy is that a pre-injection plasma is assumed to have been transported inward prior to the injection of the second component. What causes this "precursor"? If further observations verify that this plasma is always field-perpendicular, then the transportation process must act selectively upon equatorially trapped plasma alone, or off-equatorially mirroring components must have been lost in the transportation process. Plasma transport associated with magnetic impulses initiated by the IMF turnings may be important in the formation of the precursor; however, the subject is outside of our scope here.

VI. CONCLUSIONS

We have, perhaps for the first time, gathered detailed multi-satellite plasma and electric field data to make an attempt at theoretical interpretation of the observed dispersion features. We believe that, by clarifying and isolating those features attributable to adiabatic convection, the dynamical features of the injection process will surface under such an examination. The crucial result of this study is that a merger of two separately injected plasmas did occur and that the resultant plasma has lost its "memory" of the component characteristics prior to the merger. We conjecture that this is the process of formation for the *ad hoc* injection boundary, although our considerations need not be related to the *ad hoc* hypothesis to be meaningful.

REFERENCES

- Baker, D.N., T.A. Fritz, W. Lennartsson, B. Wilken, H.W. Kroehl, and J. Birn, The role of heavy ionospheric ions in the localization of substorm disturbances on March 22, 1979: CDAW 6, *J. Geophys. Res.*, **90**, 1273, 1985.
- Chiu, Y.T. and A.M. Kishi, Kinetic model of auroral plasma formation by magnetospheric convection and injection, 1. Electrons, *J. Geophys. Res.*, **89**, 5531, 1984.
- Fairfield, D.H. and A.F. Vinas, The inner edge of the plasma sheet and the diffuse aurora, *J. Geophys. Res.*, **89**, 841, 1984.
- Fennell, J.F., D.R. Croley, Jr., and S.M. Kaye, Low-energy ion pitch angle distributions in the outer magnetosphere: Ion zipper distributions, *J. Geophys. Res.*, **86**, 3375, 1981.
- Frank, L.A., J.D. Craven, C.T. Russell, and E. J. Smith, Variations of magnetotail energy in response to fluctuations of the interplanetary magnetic field, *J. Geophys. Res.* to be published, 1985.
- Ipavich, F. M., A. B. Galvin, M. Scholer, G. Gloeckler, D. Hovestadt, and B. Klecker, Suprathermal O^+ and H^+ ion behavior during the March 22, 1979 (CDAW 6) substorms, *J. Geophys. Res.*, **90**, 1263, 1985.
- Knott, K., A. Pedersen, and U. Wedeken, GEOS 2 electric field observations during a sudden commencement and subsequent substorms, *J. Geophys. Res.*, **90**, 1283, 1985.
- Koons, H.C. and J.F. Fennell, Particle and wave dynamics during plasma injection, *J. Geophys. Res.*, **88**, 6221, 1983.
- Korth, A., G. Kremser, and B. Wilken, Observations of substorm associated particle flux variations at $6 < L < 8$ with GEOS 1, *Space Sci. Rev.*, **22**, 501, 1978.
- Korth, A., G. Kremser, A. Roux, S. Perraut, J.-A. Sauvaud, J.-M. Bosqued, A. Pedersen, and B. Aparicio, Drift boundary and ULF wave generation near noon at geostationary orbit, *Geophys. Res. Lett.*, **10**, 639, 1983.
- Korth, A., G. Kremser, S. Perraut, and A. Roux, Interaction of particles with ion cyclotron waves and magnetosonic waves: Observations with GEOS 1 and 2, *Planet. Space Sci.*, **32**, 1393, 1984.

Mauk, B.H. and C.-I. Meng, Characterization of geostationary particle signatures based on the "injection boundary" model, *J. Geophys. Res.*, **88**, 3055, 1983.

McIlwain, C.E., Plasma convection in the vicinity of the geosynchronous orbit, in *Earth's Magnetospheric Processes*, edited by B.M. McCormac, p. 268, D. Reidel, Hingham, Mass., 1972.

McIlwain, C.E., Substorm injection boundaries, in *Magnetospheric Physics*, edited by B.M. McCormac, p. 143, D. Reidel, Hingham, Mass., 1974.

McPherron, R.L. and R.H. Manka, Dynamics of the 10:54 UT March 22, 1979, substorm event: CDAW 6, *J. Geophys. Res.*, **90**, 1175, 1985.

Moore, T.E., R.L. Arnoldy, J. Feynman, and D.A. Hardy, Propagating substorm injection fronts, *J. Geophys. Res.*, **86**, 6713, 1981.

Olsen, R.C., Equatorially trapped plasma populations, *J. Geophys. Res.*, **86**, 11235, 1981.

Pedersen, A., R. Grard, J. Knott, D. Jones, A. Gonfalone, U. Fahlson, Measurements of quasi-static electric fields between 3-7 Earth radii of GEOS 1, *Space Sci. Rev.*, **22**, 333, 1978.

Quinn, J.M. and R.G. Johnson, Observation of ionospheric source cone enhancements at the substorm injection boundary, *J. Geophys. Res.*, to be published, 1985.

Roux, A., S. Perraut, J.L. Rauch, and C. de Villedary, Wave-particle interactions near helium cyclotron frequency observed on board GEOS 1 and 2, 2. Generation of ion cyclotron waves and heating of helium ions, *J. Geophys. Res.*, **87**, 8174, 1982.

Russell, C.T., The ISEE 1 and 2 fluxgate magnetometers, *IEEE Trans. Geosci. Electron.*, GE-16, 239, 1978.

Shelley, E.G., R.D. Sharp, R.G. Johnson, J. Geiss, P. Eberhardt, H. Balsiger, G. Haerendel, and H. Rosenbauer, Plasma composition experiment on ISEE-A, *IEEE Trans. Geosci. Electron.*, GE-16, 266, 1978.

Stokholm, M., E. Amata, H. Balsiger, M. Candidi, S. Orsini, and A. Pedersen, Low energy ($< 130\text{eV}$) oxygen ions at the geosynchronous orbit during the CDAW 6 event of March 22, 1979, *J. Geophys. Res.*, **90**, 1253, 1985.

Strangeway, R.J. and R.G. Johnson, On the injection boundary model and dispersing ion signatures at near-geosynchronous altitudes, *Geophys. Res. Lett.*, 10, 549, 1983.

Volland, H., A semi-empirical model of large-scale magnetospheric electric fields, *J. Geophys. Res.*, 78, 171, 1973.

Young, D.T., S. Perraut, A. Roux, C. de Villedary, R. Gendrin, A.Korth, G. Kremser, and D. Jones, Wave-particle interaction near helium cyclotron frequency observed on GEOS 1 and 2, 1: Propagation of ion cyclotron waves in helium rich plasma, *J. Geophys. Res.*, 86, 6755, 1981.

LABORATORY OPERATIONS

The Aerospace Corporation functions as an "architect-engineer" for national security projects, specializing in advanced military space systems. Providing research support, the corporation's Laboratory Operations conducts experimental and theoretical investigations that focus on the application of scientific and technical advances to such systems. Vital to the success of these investigations is the technical staff's wide-ranging expertise and its ability to stay current with new developments. This expertise is enhanced by a research program aimed at dealing with the many problems associated with rapidly evolving space systems. Contributing their capabilities to the research effort are these individual laboratories:

Aerophysics Laboratory: Launch vehicle and reentry fluid mechanics, heat transfer and flight dynamics; chemical and electric propulsion, propellant chemistry, chemical dynamics, environmental chemistry, trace detection; spacecraft structural mechanics, contamination, thermal and structural control; high temperature thermomechanics, gas kinetics and radiation; cw and pulsed chemical and excimer laser development including chemical kinetics, spectroscopy, optical resonators, beam control, atmospheric propagation, laser effects and countermeasures.

Chemistry and Physics Laboratory: Atmospheric chemical reactions, atmospheric optics, light scattering, state-specific chemical reactions and radiative signatures of missile plumes, sensor out-of-field-of-view rejection, applied laser spectroscopy, laser chemistry, laser optoelectronics, solar cell physics, battery electrochemistry, space vacuum and radiation effects on materials, lubrication and surface phenomena, thermionic emission, photo-sensitive materials and detectors, atomic frequency standards, and environmental chemistry.

Computer Science Laboratory: Program verification, program translation, performance-sensitive system design, distributed architectures for spaceborne computers, fault-tolerant computer systems, artificial intelligence, micro-electronics applications, communication protocols, and computer security.

Electronics Research Laboratory: Microelectronics, solid-state device physics, compound semiconductors, radiation hardening; electro-optics, quantum electronics, solid-state lasers, optical propagation and communications; microwave semiconductor devices, microwave/millimeter wave measurements, diagnostics and radiometry, microwave/millimeter wave thermionic devices; atomic time and frequency standards; antennas, rf systems, electromagnetic propagation phenomena, space communication systems.

Materials Sciences Laboratory: Development of new materials: metals, alloys, ceramics, polymers and their composites, and new forms of carbon; non-destructive evaluation, component failure analysis and reliability; fracture mechanics and stress corrosion; analysis and evaluation of materials at cryogenic and elevated temperatures as well as in space and enemy-induced environments.

Space Sciences Laboratory: Magnetospheric, auroral and cosmic ray physics, wave-particle interactions, magnetospheric plasma waves; atmospheric and ionospheric physics, density and composition of the upper atmosphere, remote sensing using atmospheric radiation; solar physics, infrared astronomy, infrared signature analysis; effects of solar activity, magnetic storms and nuclear explosions on the earth's atmosphere, ionosphere and magnetosphere; effects of electromagnetic and particulate radiations on space systems; space instrumentation.

...

END

2-87

DTIC